MARCHE POLYTECHNIC UNIVERSITY

DEPARTMENT OF LIFE AND ENVIRONMENTAL SCIENCES

Master Degree Course in Marine Biology

Caratterizzazione della fotosintesi e dell'allocazione del carbonio in specie di microalghe marine acclimatate a diversi regimi di illuminazione

Characterization of photosynthesis and carbon allocation in marine microalgal species acclimated to different light regimes

Master Degree Thesis by:

Aja Trebec

Relator: Chiar.mo Prof. Alessandra Norici

Co-relator: Dott.Caterina Gerotto

Session: February

Academic Year: 2019/2020

To my mother

INDEX

LIST OF FIGURES

LIST OF TABLES

ABSTRACT

Marine microalgae are a heterogeneous group of photosynthetic autotrophs. In addition to providing almost half of the oxygen on Earth, these organisms are extremely important carbon fixators. Their capability to live in a wide range of environments, and thus, tolerate a huge range of physical and chemical conditions, makes them great organisms to study. Here, we explore what occurs when marine microalgae from the green evolutionary lineage, such as *Tetraselmis suecica* and *Dunaliella salina*, and from the red lineage, such as *Phaeodactylum tricornutum*, are exposed to different light regimes. Light influences the photosynthetic reactions and the metabolic pathways within cells. To overcome any difficulties, marine microalgae have to counter-act the potential stressful impacts, and they do so by photoacclimating, or photoadapting, depending on whether the impact lasts from hours to days, or days to months, respectively.

Microalgal species *Tetraselmis suecica, Dunaliella salina* and *Phaeodactylum tricornutum* were grown in batch cultures. "Control" conditions (CTR) corresponded to continuous light (24h) and light intensity of 100 μmol photons·m^2·s^{-1}. "Low light" conditions (LL) corresponded to continuous light (24h) and 10 μmol photons·m^2·s^{-1}, and in the third light condition, algae were exposed to 12 hours light and 12 hours dark with light intensity of 100 μmol photons·m^2·s^{-1}, thus, the "photoperiod" conditions (PP).

Through the observed process of photoacclimation, the maximum growth rate is the greatest in all species under CTR conditions, and the most pronounced in the diatom *P. tricornutum*, that is also the species with the smallest dimensions. While the amount of carbohydrates under LL conditions diminishes in *T. suecica* and *D. salina,* it was not the case for *P. tricornutum.* Proteins substantially increase in all species acclimated to LL compared to the CTR. Giving the concomitant 2-fold increase of chlorophyll pigments and significantly higher photosynthetic efficiency for the photon capture in LL, we can conclude that cells acclimate by amplifying their photosynthetic apparatus (more abundant photosystems and antenna proteins). However, *D. salina* accumulates the most

proteins under PP conditions. The lipids content increases in *T. suecica* and *P. tricornutum*, but in *D. salina*, it stays unvaried among all conditions.

By examining the kinetics of photosynthesis, *D. salina* and *P. tricornutum* CTR have a higher non-photochemical quenching (NPQ) upon increasing illumination, while in *T. suecica*, NPQ is low. Additionally, the different parameters analysed for the characterization of the photosynthetic response show a peculiar kinetics in *D. salina*, hence leading to think that there is a complex control of the electronic transport.

Physiological differences observed in the applied light conditions, both at a specific and interspecific level, have allowed to confirm the extreme diversification of the physiological responses of microalgae to environmental conditions, opening new possibilities of research, useful for a greater understanding of photosynthesis and metabolism in the different microalgal species.

RIASSUNTO

Le microalghe marine sono un gruppo eterogeneo di organismi fotoautotrofi. Oltre a fornire quasi la metà dell'ossigeno sulla Terra, questi organismi sono degli ottimi fissatori di carbonio. La loro capacità di vivere in una vasta gamma di ambienti e, quindi, tollerare diverse condizioni fisiche e chimiche, li rende ottimi organismi da studiare. Questa tesi vuole esplorare cosa accade quando microalghe marine della linea evolutiva verde, come *Tetraselmis suecica* e *Dunaliella salina*, e della linea rossa, come *Phaeodactylum tricornutum*, sono esposte a diversi regimi di illuminazione. La luce influenza le reazioni fotosintetiche e le vie metaboliche all'interno delle cellule. Per superare qualsiasi problema legato alla disponibilità di luce, le microalghe marine devono fotoacclimatarsi o fotoadattarsi, a seconda che l'impatto duri rispettivamente da ore a giorni o da giorni a mesi. Attraverso il processo di fotoacclimatazione qui osservato, le diverse specie algali modificano l'apparato fotosintetico e il pool macromolecolare in modo differenziato, nelle condizioni di luce applicate. I risultati qui riportati possono servire come un ottimo strumento per una ricerca più approfondita e lo sviluppo di future applicazioni biotecnologiche.

In particolare, le specie *T. suecica*, *D. salina* e *P. tricornutum* sono state cresciute in colture batch e sottoposte a tre diverse condizioni di illuminazione. La condizione "controllo" (CTR) corrisponde a un'illuminazione continua (24h) con intensità 100 μmol fotoni·m^2·s^{-1}; la condizione "bassa luce" (LL) ad una illuminazione di 24h con intensità 10 μmol fotoni·m^2·s^{-1}; e condizione "fotoperiodo" (PP) è caratterizzata dalla presenza del fotoperiodo di 12 ore di luce e 12 ore di buio, con intensità 100 μmol fotoni·m^2·s^{-1}.

I tassi di crescita massimi di tutte le specie algali sono più alti nei CTR, il tasso in assoluto più alto è osservato nella diatomea *P. tricornutum*, caratterizzata dalle dimensioni cellulari minori. L'acclimatazione alle diverse condizioni di crescita è analizzata tramite caratterizzazione della quota cellulare di C ed N, della composizione dei principali pool macromolecolari (proteine, carboidrati, lipidi), così come mediante la caratterizzazione della fotosintesi, in campioni appartenenti alla fase

di crescita medio esponenziale. In cellule di CTR, la biomassa è circa 20% più alta rispetto a cellule acclimatate a LL in *T. suecica* e *D. salina.* Inoltre, anche il contenuto di carbonio è maggiore nel CTR. La quantità di carboidrati nelle alghe verdi è circa la metà in LL rispetto alla quantità nel CTR, mentre in cellule di *T. suecica* PP, il pool dei carboidrati è simile a quello del CTR. *P. tricornutum*, invece, accumula più carboidrati proprio in LL. Il pool delle proteine è molto più alto in tutte le specie cresciute a LL. Visto il parallelo incremento dei pigmenti fotosintetici e la maggiore efficienza fotosintetica per la cattura di fotoni in LL, si può concludere che le cellule si acclimatano ampliando il loro apparato fotosintetico (più abbondanti fotosistemi e proteine antenna). Il pool dei lipidi è altamente modificato in *P. tricornutum*, mentre in *D. salina* la quantità di lipidi non è influenzata dalle condizioni studiate. Studiando la cinetica fotosintetica, si è visto che in CTR, *D. salina* e *P. tricornutum* mostrano un NPQ molto più alto quando illuminate con intensità luminose crescenti, mentre in *T. suecica*, l'NPQ è più basso. In *D. salina*, la risposta fotosintetica mostra una cinetica peculiare, che suggerisce la presenza di un controllo molto complesso del trasporto elettronico.

Differenze fisiologiche osservate nelle condizioni di illuminazione applicate, sia a livello specifico che interspecifico, hanno permesso di confermare l'estrema variabilità delle risposte fisiologiche delle microalghe alle condizioni ambientali, aprendo nuove line di ricerca, utili ad una maggiore comprensione della fotosintesi e del metabolismo nelle diverse specie microalgali.

INTRODUCTION

1.1. Experimental species

The characterization of photosynthesis and the allocation of carbon is investigated in three marine microalgal species acclimated to different light conditions. The species considered are two green microalgae *Tetraselmis suecica* and *Dunaliella salina*, and a brown microalgae *Phaeodactylum tricornutum* (Table 1).

Table 1. Taxonomy of algal species from algaebase.org.

Species	Family	Order	Class	Phylum
Tetraselmis suecica	Chlorodendraceae	Chlorodendrales	Chlorodendrophyceae	Chlorophyta
Dunaliella salina	Dunaliellaceae	Chlamydomonadales	Chlorophyceae	Chlorophyta
Phaeodactylum tricornutum	Phaeodactylaceae	Bacillariophyta ordo incertae sedis	Bacillariophyta classis incertae sedis	Bacillariophyta

1.1.1. Tetraselmis suecica

The marine unicellular species *Tetraselmis suecica* belonged to the class of Prasinophyceae in the past (Fabregas et al., 1984). However, being a marine scaly quadriflagellate, together with unicellular algal species of the genus Scherffelia, it is now classified into a small clade of Chlorodendrophyceae. This clade is in close relationship with the green algae of Ulvophyceae, Trebuxiophyceae and Chlorophyceae (UTC) clades because of the closed mitosis and the presence of a phycoplast (Leliaert et al., 2012).

The species possesses four hair-covered flagella. These flagella are also scaly. It has a rigid extracellular wall that covers not only the protoplast surface, but also the apical depression, known as the pit, too (Domozych et al., 1981). The cell wall has been considered as a theca in some scientific papers (Manton & Parke, 1965) and it develops from small stellate particles released from the vesicles of the Golgi apparatus.

The ability of *Tetraselmis suecica* to grow under different nutrient and salinity concentrations (Sen et al., 2005) has made it important, ecologically and commercially. In the latter case, this species is used as live feed in aquaculture (Borghini et al., 2009). Moreover, *Tetraselmis suecica* could be used for supplement and cosmetic production for humans due to the fact that it accumulates high quantities of α-tocopherol (vitamin E), especially during the exponential growth phase (Carballo-Cárdenas et al., 2003).

1.1.2. Dunaliella salina

Dunaliella salina is a unicellular green algae belonging to the phylum of Chlorophyta. It is considered a model photosynthetic eukaryote, widely studied for its capacity to acclimate to stressful conditions, tolerate high salinity concentrations, and accumulate carotenoids (Zhao et al., 2011). Due to the fact that *Dunaliella salina* can grow in such extreme environmental conditions, and because of a distinct morphological characteristic, it has challenged taxonomists in classifying it properly (Borowitzka & Siva, 2007). In fact, the genus Dunaliella is characterised by the lack of a cell wall (OLIVEIRA et al., 1980) and the presence of a glycoprotein cell coat that allows this genus to tolerate osmotic stress (Einspahr et al., 1988).

The marine microalgae *Dunaliella salina* is biflagellate, ovoid to cylindrical, and under stress conditions changes its form to bilateral, or even asymmetrical. The cell width ranges from 7,9 to 13,2 μm (Borowitzka & Siva, 2007).

Under high light intensities, *Dunaliella salina* accumulates β-carotenes to such extent that the production of these pigments is one to two orders of magnitude larger than that of commercially exploited β-carotene plant producers (Lamers et al., 2010). Light, indeed, plays an important role in the biosynthesis of the stereo-isomeric form of beta-carotene, known as 9-cis-beta-carotene (Cowan et al., 1992). The higher the light intensity, the higher is the production of 9-cis-beta-carotene by *Dunaliella salina*.

1.1.3. Phaeodactylum tricornutum

Phaeodactylum tricornutum was described by Bohlin in 1898. This species is a marine microalgae characterised by a silica frustule, which is a shell-like structure typical of the phylum Bacillariophyta, or else known as diatoms. *Phaeodactylum tricornutum* is the only pennate species that belongs to the family Phaeodactylaceae and genus Phaeodactylum (LEWIN, 1958). In comparison to the other diatoms that have a two valve silicified frustule, *Phaeodactylum tricornutum* possesses only one valve, whereas the rest of the cell wall is unsilicified (Bowler & Falciatore, 2019).

It is a rather important eukaryotic unicellular species, since together with other diatoms, it is responsible for one-fifth of the photosynthesis on Earth (Armbrust, 2009). Not only is *Phaeodactylum tricornutum* involved in the ocean carbon sink (Geider et al., 2001), but its cultivation serves as food in aquaculture having been able to produce eicosapentaenoic acid (EPA) (Jiang & Gao, 2004).

1.2. Photosynthesis

Life on Earth would not be possible without the energy coming from the sun. The photon energy or light represents the driving factor of photosynthesis (Ecology, 2008), a complex set of reactions that occur in photosynthetic organisms. Evolutionary speaking, oxygenic photoautotrophs had most

probably evolved as much as 2.7 billion years ago (Buick, 2008). These formidable organisms are able to synthesize complex carbon compounds from the mere use of solar energy.

In eukaryotic species, the process is carried out in photosynthetic plastids (chloroplasts), that are endosymbiotic organelles derived from the incorporation of a cyanobacterium into an eukaryotic host. In fact, this symbiotic event is called primary endosymbiosis. However, plastids may be formed also through secondary and tertiary endosymbioses, which happen when a second eukaryotic host incorporates an eukaryotic algae containing plastids (Moreira & Philippe, 2001). Depending on how many endosymbiotic events organisms undergo, different taxa can be distinguished as follows in Table 2.

Table 2. Endosymbiotic events in different algal taxa. In green are represented green algae, such as *Tetraselmis suecica* and *Dunaliella salina*. In orange are shown algae belonging to Ochrophyta and heterokonts, under which diatoms, including *Phaeodactylum tricornutum*, are currently classified. Table modified from Howe et al., 2008.

group	primary, secondary or tertiary	presence of chlorophylls and/or phycobiliprotein	no. of surrounding membranes
green plants/algae	1°	chlorophyll *a*, *b*	2
red algae	1°	chlorophyll *a*, phycobiliprotein	2
Glaucophyta	1°	chlorophyll *a*, phycobiliprotein	2
Cryptophyta	2°	chlorophyll *a*, *c* phycobiliprotein	4
Chlorarachniophyta	2°	chlorophyll *a*, *b*	4
Ochrophyta and heterokonts	2°	chlorophyll *a*, *c*	4
Haptophyta	2°	chlorophyll *a*, *c*	4
Euglenophyta	2°	chlorophyll *a*, *b*	3
dinoflagellates	2°, 3°	mostly chlorophyll *a*, *c*	3
Apicomplexa	2°	none	4

Oxygenic photosynthesis takes place through two sets of reactions, that are light and so-called “dark” reactions. Two water molecules are split using the photon energy into oxygen, protons and electrons in the light reactions. Protons and electrons are used for the production of ATP and NADPH. The latter two products are then used in the dark reactions, to reduce CO_2 to carbohydrate (Johnson, 2016).

1.2.1. Pigments

Photosynthetic plastids, or chloroplasts, are found among eukaryotic algae. These organelles are formed through primary endosymbiosis in green algae, and confine photosynthetic pigments chlorophylls *a* and *b*. As seen in Figure 1, the molecular structure of chlorophyll *a* consists in a closed tetrapyrrole ring with a magnesium ion at the centre (Björn et al., 2009). These chlorophylls are present in *Tetraselmis suecica* and *Dunaliella salina*, whereas *Phaeodactylum tricornutum* contains secondary plastids that are formed through secondary endosymbiosis, are surrounded by four membranes and hold chlorophylls *a* and *c* (Dougherty et al., 1970). Chlorophyll *c* molecular structure has a porphyrin nucleus (Granick, 1965).

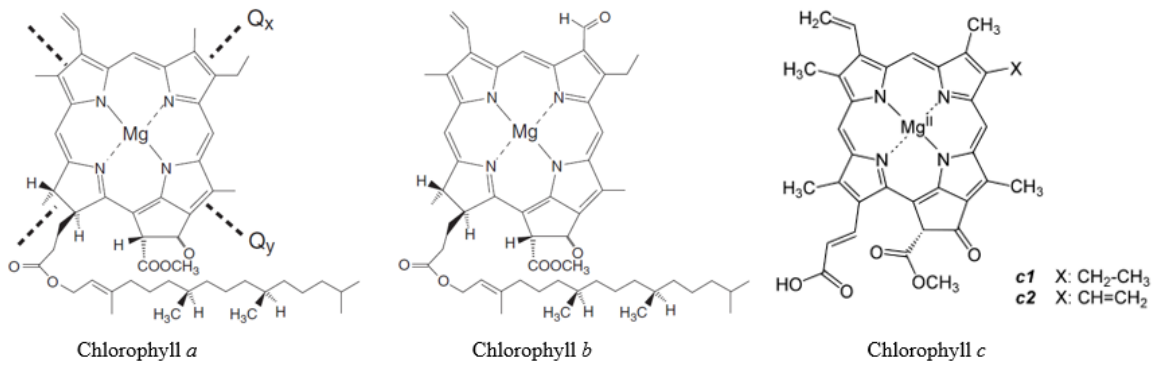

Figure 1. The molecular structure of chlorophylls *a*, *b* and *c*. Image modified from Chen & Blankenship, 2011.

Chlorophyll *a* (Chl *a*) is always present, being enclosed in the "special pairs," the reaction centre pigments able to convert the energy of absorbed photons into chemical energy (Björn et al., 2009). Two (or more in secondary endosymbionts) membranes enclose the stroma compartment, where the C fixation reactions occur, and, contain thylakoids, membranes in which the main protein complexes driving light-dependent reactions of photosynthesis are localized (Figure 2). The thylakoid membrane surrounds the lumen compartment.

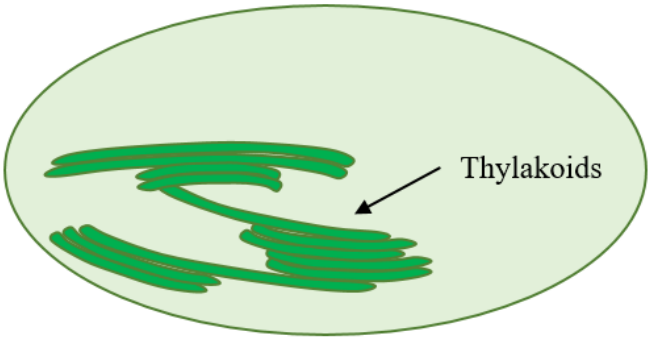

Figure 2. Schematic chloroplast structure of a green algae containing thylakoids.

As previously discussed, pigments take up light energy and perform a series of light driven redox reactions, so to produce a proton motive force for ATP production and reduce molecules for CO_2 fixation (Hamilton, 2019). Although light is essential, when too high, it can lead to oxidative damage. Hence, along with chlorophylls and quinones present in the photosynthetic machinery (MacIntyre et al., 2002), photoautotrophic organisms have evolved various types of accessory pigments, both photoprotecting and photosynthetic. Photoprotective carotenoids (PPC), for instance, protect chlorophyll from photo-oxidation by absorbing the excessive quanta that are not involved in the photosynthetic reactions (Ficek et al., 2000). As a result, oxygenated carotenoids, or xanthophllys, undergo non-photochemical quenching. In other words, the excessive energy is dissipated as heat through the xanthophyll cycle (Álvarez et al., 2019) that will be discussed briefly.

1.2.2. Light as a particle and a wave

The radiant energy of light is a particle, known as a photon, that holds a certain quantity of energy or quantum. Despite being a particle, light is also an electromagnetic wave, and thus has a wavelength (λ) (Mccree, 1981). The shorter the wavelength of a photon, the higher is its energy.

During photosynthesis, only wavelengths (λ) between 400 and 700 nm get absorbed by pigments, mainly chlorophylls, and that is called the photosynthetically active radiation (PAR) (Cardona et al., 2018; Figure 3).

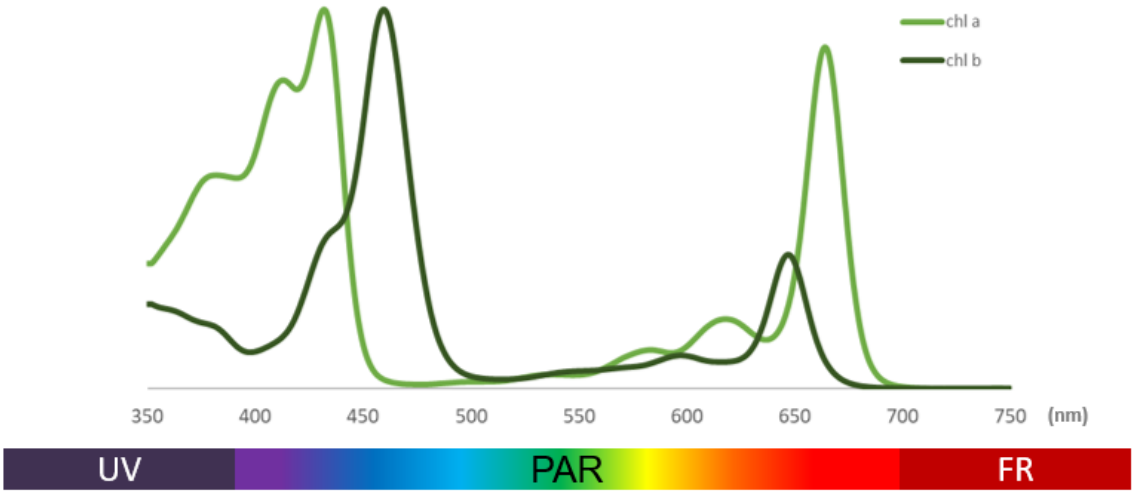

Figure 3. Electromagnetic spectrum in the wavelength range between 350 and 750 nm includes the UV, visible and the near IR. The human eye can see in a narrow range of wavelengths of radiation, that extends from 400 nm (violet) to 700 nm (red), and hence, called the visible range. Pigments absorb wavelengths in this range that represents the photosynthetically active radiation (PAR). The absorption spectra of Chl *a* and Chl *b* are shown with light green and dark green curves, respectively.

1.2.3. Light reactions

The capture of light energy occurs in the thylakoid membranes of chloroplasts, where photosystems (PS) are found. These complexes consist of clustered photosynthetic pigments. The PSII and PSI have light harvesting chlorophylls and other pigments that funnel the light energy to their reaction centres. A chlorophyll molecule makes a transition from its ground energy state to its excited state when hit by a photon. Thus, being unstable, it has to convert back to the ground state (Taiz & Zeiger, 2010). Firstly, it can relax through fluorescence, by emitting a photon. Secondly, it can return to the lowest excitation state by dissipating heat. Thirdly, it can fuel photosynthetic reactions through

photochemistry (Müller et al., 2001). In particular, PSII and PSI absorb wavelengths around 680 and 700 nm, respectively, and are at large considered as P680 and P700 (Barber & Archer, 2001). The light reactions depend on these membrane embedded photosystems, because they carry out a linear electron transfer, at the end of which NADPH is produced (Larkum, 2003).

Around the abovementioned photosystems, light harvesting complexes (LHC) I and II are found (Green et al., 2003; Figure 4). The LHCs contain pigments that capture and transfer the photon energy that serves as charge separation in the PSI and PSII. Therefore, LHCs are important in terms of photosynthetic efficiency. The outermost and most abundant antenna complex, the LHCII, binds the large majority of all chlorophyll on Earth (Croce et al., 2001).

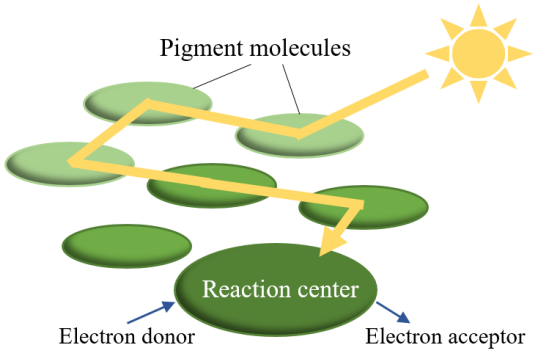

Figure 4. A scheme of energy transfers during photosynthesis. Light is absorbed by pigment molecules that compose the antenna complex. This energy transfer goes all the way to the reaction centre, where it becomes an electron transfer, in which an electron donor gives up electrons to an acceptor.

Besides having the PS complexes, the thylakoid membrane of a chloroplast has two other protein complexes that are the cytochrome b_6f and ATP synthase. All four embedded complexes, together with the PSII and PSI, work synergistically and perform a series of redox reactions (Figure 5).

When chlorophyll molecules in the PSII are hit by light energy, these chlorophylls get excited and pass their excitation energy to the reaction centre molecule. The electrons are passed from PSII to the electron transport chain. In parallel, the lost electrons by PSII are replaced by electrons coming from a process called photolysis (Rutherford & Boussac, 2004). A water molecule, that is the main

electron donor, is oxidized by the protein D1 found in PSII, where molecular oxygen (O_2) is produced as a by-product and four protons are released (Kim et al., 1993).

The electrons form PSII are passed through a quinone pool and the cytochrome b_6f protein complex to a small soluble, copper-containing protein called plastocyanin. When the PSI absorbs the solar energy, an electron is translocated from plastcynanin on the luminal side to the ferredoxin on the side of the thylakoid stroma. Hence, the reduced ferredoxin is used by the ferredoxin-NADP reductase for NADPH production (Nelson & Ben-shem, 2015). In other words, the build-up of two electrons and one proton is stored in the formation of NADPH molecule from $NADP^+$ on the side of the stroma. Meanwhile, the electrons that are lost by the PSI are replaced by electrons generated in the PSII.

The cytochrome b_6f constantly reduces the plastoquinone on the stomatal side and oxidizes it on the luminal side in a process called the Q cycle (Mitchell, 1975). This results in a build-up of protons in the thylakoid lumen, which generates a proton motive force (pmf) across the membrane, that is utilised by ATP synthase, the fourth protein complex, to synthesize adenosine triphosphate (ATP) (Sheng et al., 2019), the main energy currency of the cell, that is released in the chloroplast stroma. This energy coin is synthesized from adenosine diphosphate (ADP) and orthophosphate (Pi) through photophosphorylation, where fourteen protons (H^+) are needed to produce three molecule of ATP (Kramer & Evans, 2011).

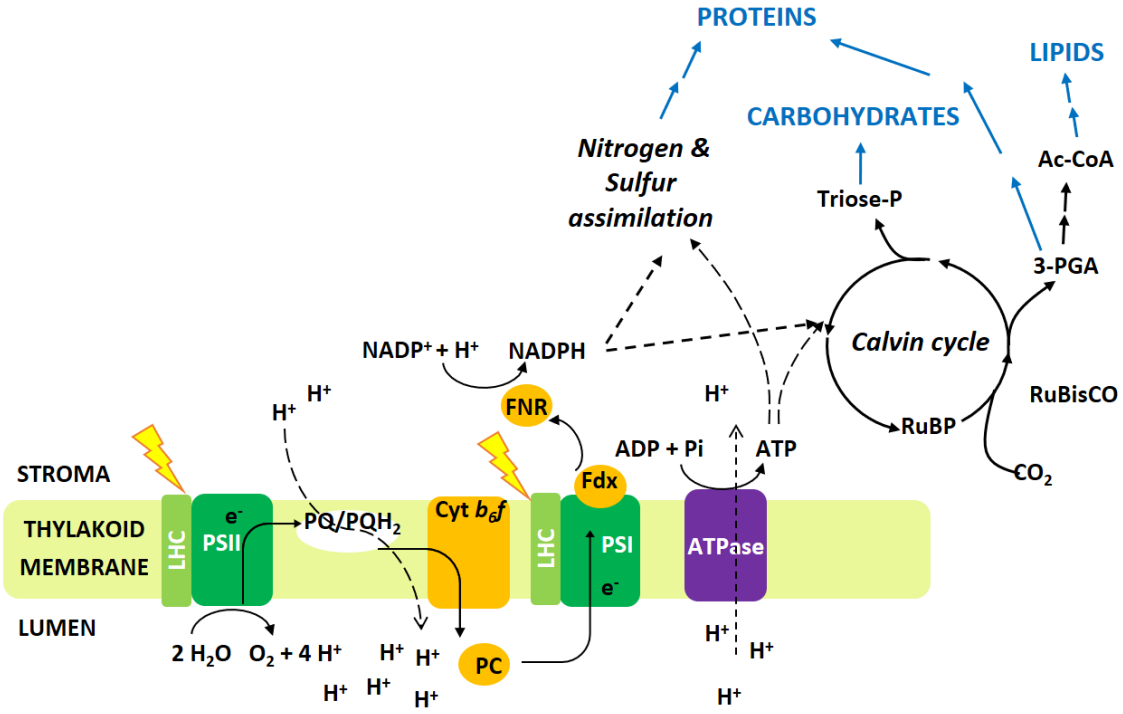

Figure 5. Schematic representation of the chloroplast photosynthetic apparatus of the green algae. The diagram represents the thylakoid membrane with the four major supercomplexes, the electron transport chain, and the further use of products of the light reactions for the dark reactions (Calvin cycle) and other metabolic pathways.

1.2.4. Dark reactions

ATP and NADPH free energy molecules produced during the light reactions are released in the stomatal side of the thylakoid, where they are furtherly used in the assimilation of CO_2, also known as dark reactions or Calvin-Benson cycle (Buchanan, 2016). These reactions occur in the presence of one of the most abundant enzymes on the planet, called ribulose-1,5-bisphosphate carboxylase/oxygenase (RuBisCO). Thanks to several reactions, three molecules of CO_2 are reduced to one molecule of glyceraldehyde 3-phosphate (G3P), with a net consumption of nine molecules of ATP and six molecules of NADPH. Two G3P molecules are needed for the production of one molecule of glucose that is used by the cell for further reactions. Analogously, ribulose bisphosphate

(RuBP) is regenerated for the following CO_2 assimilation of the Calvin-Benson cycle (Sharkey, 2019). In addition, the energy molecules produced from the light reactions are not only used in the Calvin-Benson cycle, but also in other metabolic pathways involved in the production of macromolecules, such as carbohydrates, proteins and lipids (Figure 5).

1.2.5. Acclimation to light in the sea

Microscopic marine algae live in a rather wide range of marine environments, either in colonies, attached to the sediment or other organisms, or as free-living cells in the water column. In the third instance, they make part of the phytoplankton. Moving freely, the phytoplankton is subject to vertical transport through the euphotic zones (upper 200 meters) of the ocean, and therefore, to short-term changes in irradiance (Olaizola et al., 1994). In order to successfully photosynthesise and survive, marine microalgae must photoacclimate, which happens in a time range from hours to days. Hence, they must increase the synthesis of light-harvesting pigments, such as chlorophylls in the case of *Tetraselmis suecica* and *Dunaliella salina* and photosynthetic accessory pigment called fucoxanthin in the case of *Phaeodactylum tricornutum* (Owens, 1986), under dim light. This ensures them an efficient utilisation of that small amount of light through absorption of photons that cannot be captured by the Chl *a*. Conversely, the abovementioned pigments decrease under supraoptimal irradiance, whereas the synthesis of photoprotective pigments, as those of the xanthophyll cycle, increases.

Last but not least, another consequence of acclimation is the change in size of the light harvesting pigment antennae by means of changes in gene expression or proteolysis. Thus, the antennae become larger in dim light and smaller under high light (Neidhardt et al., 1998).

1.2.6. Protective mechanisms

Photosynthetic oxygenic organisms, including microalgae, can grow and thrive at a wide range of light intensities due to different photosynthetic regulation and acclimation mechanisms, including the xanthophyll cycles (Sharma et al., 2012). By photoacclimating, photoautotrophs, regulate the amount of pigments and other components of the photosynthetic apparatus. In chlorophytes, the pigments involved in the xanthophyll cycle are zeaxannthin, violaxanthin and antheraxantin, whereas in diatoms (Bacillariophyceae), they are replaced by diadinoxanthin and diatoxanthin (Dubinsky & Stambler, 2009).

Under increasing light intensities, violaxanthin is converted into antheraxanthin, and the latter into zeaxanthin, by means of two de-epoxidation reactions, shown in Figure 6A. On the contrary, when light decreases, zeaxanthin is first epoxidised into antheraxanthin, and then into violaxanthin. These cyclic reactions take place thanks to the enzymes violaxanthin de-epoxidase and zeaxanthin epoxidase (Iii, 1973). The former enzyme functions properly under low pH and high light conditions. In each step, it removes an epoxide group by involving an ascorbate and NADPH as reductants. Zeaxanthin epoxidase, on the other hand, utilises O_2 and NADPH as oxidants for the formation of violaxanthin, and it is favoured under limiting light and a higher pH.

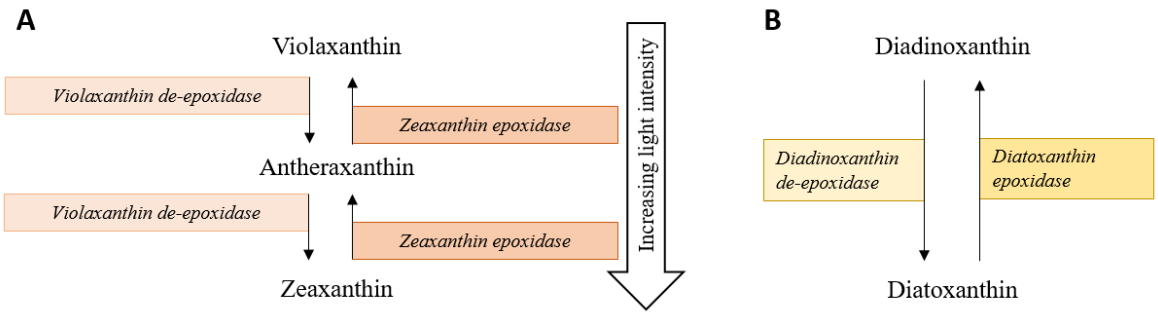

Figure 6. The scheme represents the xanthophyll cycle typical for Chlorophytes (A). The diadinoxanthin cycle occurs in microalgae belonging to the group Bacillariophyta, or diatoms (B).

However, the contribution of the xanthophyll cycle in dissipating energy varies notably among different species of microalgae of the phylum Chlorophyta (Torzillo et al., 2004), therefore, it might be possible that green microalgae poses other additional dissipation mechanisms involved in heat dissipation, the fast, pH-dependent and, usually, main component of non-photochemical quenching. As a matter of fact, green microalgae accumulate light harvesting complex stress related (LHCSR) proteins upon higher light intensities (Peers et al., 2009). These proteins belong to the LHC family and are activated by changes in the thylakoid luminal pH.

Unlike green algae, as shown in Figure 6B, diatoms convert diadinoxanthin into its de-epoxidised form, called diatoxanthin, by means of the diadinoxanthin de-epoxidase under high light (Goss et al., 2006). In addition to the diatoxanthin, LHCX proteins found in diatoms provide the capacity to rapidly dissipate the excessively absorbed energy under the form of heat (Buck et al., 2019). These proteins are similar to LHCSR proteins found in green algae.

Although microalgae are capable of counteracting the stress caused by high irradiance through photoacclimation, when the irradiance is excessive, some of the key proteins of the photosynthetic machine (e.g. D1 protein of PSII) get damaged by photoinhibition. Thus, the photosynthetic yield is lost, and the growth rate decreased (Hartmann et al., 2013; Raven, 2011).

MATERIALS AND METHODS

2.1. Algal cultures

2.1.1. AMCONA medium

Seawater medium was prepared according to the laboratory protocol for Artificial Multipurpose COmplement for the Nutrition of Algae (AMCONA medium).

Table 3. Recipe for Artificial Multipurpose COmplement for the Nutrition of Algae (from internal laboratory protocol).

Chemical substance	**Stock [ ]**	**Final [ ]**	**Volume for 1 L**
NaCl		363 mM	21.21 g
Na_2SO_4	1 M	25 mM	25 mL
KCl	1.6 M	8.04 mM	5 mL
$NaHCO_3$	0.41 M	2.07 mM	5 mL
KBr	3.63 M	725 µM	0.2 mL
H_3BO_3	0.37 M	372 µM	1 mL
NaF	0.33 M	65.7 µM	0.2 mL
$MgCl_2 \cdot 6H_2O$	1.65 M	41.2 mM	25 mL
$CaCl_2 \cdot 2H_2O$	1.83 M	9.14 mM	5 mL
$SrCl_2 \cdot 6H_2O$	0.41 M	82 µM	0.2 mL
$NaNO_3$	2.74 M	549 µM	0.2 mL
$NaH_2PO_4 \cdot H_2O$	100 mM	21 µM	0.21 mL
$Na_2SiO_3 \cdot 9H_2O$	205 mM	205 µM	1 mL
$CuSO_4 \cdot 5H_2O$	40 µM	40 nM	1 mL
METAL SOLUTION	6.5 mM	6.56 µM	1 mL

I- Iron METAL SOLUTION II- Trace Metal			1 mL
TRIS-HCl; pH=8.1	1 M	10 mM	10 mL
VITAMINS SOLUTION			1 mL

METAL SOLUTIONI- Iron [1 mL L^{-1}] 6.56 mM

Chemical substance	**gL^{-1} stock solution**
$FeCl_3 \cdot 6H_2O$	1.77
$Na_2EDTA \cdot 2H_2O$	3.09

METAL SOLUTION II- Trace Metal [1 mL L^{-1}]

Chemical substance	**gL^{-1} stock solution**	**Final concentration**
$ZnSO_4 \cdot 7H_2O$	0.073	254 nM
$CoSO_4 \cdot 7H_2O$	0.016	5.69 nM
$MnSO_4 \cdot 4H_2O$	0.54	2.42 μM
$Na_2MoO_4 \cdot 2H_2O$	1.48×10^{-3}	6.1 nM
Na_2SeO_3	1.73×10^{-4}	1 nM
$NiCl_2 \cdot 6H_2O$	1.49×10^{-3}	6.3 nM
$Na_2EDTA \cdot 2H_2O$	2.44	8.29 μM

VITAMIN STOCK [1 mL L^{-1}]

Vitamin	**gL^{-1} stock solution**	**Final concentration**
Thiamine-HCl	0.1	297 nM
Biotin	0.002	4.09 nM
B_{12}	0.001	1.47 nM

2.1.2. Growth conditions

Control culture (hereafter, CTR) were grown at a temperature of 20°C, continuous light and photon flux density (PFD) equal to 100 µmol·m^2·s^{-1} (Sanyo fluorescent lamp). Low light (LL) acclimation was obtained by covering flasks with a grey plastic mesh to decrease the light intensity to 10 µmol·m^2·s^{-1}. A third set of samples were cultured at the same temperature and photon flux density as CTR but with a photoperiod of 12h light:12h dark, thus signed as PP.

Experimental cultures of *Tetraselmis suecica* (CCAP 66/4), *Dunaliella salina* (CCAP 19/25) and *Phaeodactylum tricornutum* (UTEX 646) were inoculated from pre-inoculums in exponential growth phase.

2.1.3. Inoculums

100 µL of each pre-inoculum were mixed with a 10 mL CASYTon solution and counted with CASY® cell counter. Based on the result given by the counter, the following equation was used:

$c_i \cdot V_i = c_f \cdot V_f$;

in order to determine the volume (V) needed to prepare 100 mL of inoculum cultures containing $2{,}5 \cdot 10^5$ cells. The calculation was therefore the following:

$V_i = \frac{c_f \cdot V_f}{c_i} = \frac{2{,}5 \cdot 10^5 cells \cdot 100mL}{c_i}$;

where c_i is the concentration given by the CASY® cell counter. The obtained volume for each species was taken from pre-inoculums and put into sterile plastic falcon tubes under the biological safety cabinet. Pre-inoculums were centrifuged at 4500 g for 10 minutes. Afterwards, the supernatant was removed with a pipette under sterile conditions. The centrifuged cells were resuspended in 10 mL AMCONA medium. Each resuspended algal culture was added to 90 mL AMCONA medium

contained in 250 mL Erlenmeyer flasks. The Erlenmeyer flasks were stirred gently, in a circular way. 150 μL were again taken from each inoculum and used for cell counting in the same way as mentioned earlier. This step was done in order to be sure that the cell concentration inoculated was right and to obtain the "day 0" measurement for the growth curve. Lastly, inoculums were placed into the culture growth chambers in CTR, LL or PP conditions as described above.

Growth (cell density) was followed for 12 days by counting daily cell number with the aid of CASY-TT automated cell counter. Experiments to characterize microalgae physiology in the different light conditions were conducted on cells from the mid exponential phase.

2.2. Quantification of pigments

The quantification of pigments was done by taking 2 mL of mid-exponential phase culture from each algal species and condition. This volume was centrifuged at 4500 *g* for 10 minutes. After the centrifugation, the supernatant was thrown away. 1 mL of acetone 90% was quickly added to pellets of both *Tetraselmis suecica* and *Dunaliella salina*. *Dunaliella salina* samples were freezed overnight at -20°C, whereas *Tetraselmis suecica* samples were placed in the fridge for a couple of days and then moved to the freezer for optimal pigment extraction.

Samples of the diatom *Phaeodactylum tricornutum* were treated differently. 1 mL of methanol alcohol was added to each pellet, gently resuspended and then placed into the freezer overnight at -20°C.

Effective extraction of pigments was verified prior to spectrophotometric quantification by checking the pelleted insolubilized material, containing e.g. proteins, to be white.

After extraction of pigments, each sample was centrifuged at 4500 *g* for 10 minutes. The supernatant was transferred into another sterile Eppendorf tube and placed in the dark, in order to prevent any pigment degradation due to light exposure.

The blank was performed with 700 µL of either acetone 90% or methanol, depending on the species analysed, that were put into the quartz cuvette.

Firstly, the absorbance value of the 730 nm wavelength was subtracted to the absorbance of other wavelengths.

Secondly, in order to calculate the concentrations of pigments, absorbance coefficients (E_λ) shown in Table 4 were taken into consideration for the subsequent spectrophotometric equations found below (Ritchie, 2006).

Table 4. Absorbance coefficients for spectrophotometric equations from Ritchie, 2006.

Extracting solution	Organisms	Pigment	Abbrev	Abs. Peak (nm)	E_λ
Acetone 90%	Chlorophytes	Chlorophyll *a*	Chl *a*	664	11,8668
				647	-1,7858
		Chlorophyll *b*	Chl *b*	664	-4,895
				647	18,9775
Methanol	Diatoms and phaeophytes	Chlorophyll *a*	Chl *a*	664	13,2654
				630	-2,6839
		Chlorophyll $c_1 + c_2$	Chl $c_1 + c_2$	664	-6,0138
				630	28,8191

In the case of *Tetraselmis suecica* and *Dunaliella salina*, calculations were proceeded as follows:

$$Chlorophyll\ a\ (\mu g/mL) = (-1{,}7858 \cdot A_{647}) + (11{,}8668 \cdot A_{664})$$

$$Chlorophyll\ b\ (\mu g/mL) = (18{,}9775 \cdot A_{647}) - (4{,}895 \cdot A_{664})$$

As for *Phaeodactylum tricornutum*, the equations were slightly changed because methanol was used as the extracting solution instead of acetone 90%:

$$Chlorophyll\ a\ (\mu g/mL) = (-2{,}6839 \cdot A_{630}) + (13{,}2654 \cdot A_{664})$$

$$Chlorophyll\ c_1 + c_2\ (\mu g/mL) = (28{,}8191 \cdot A_{630}) - (6{,}0138 \cdot A_{664})$$

Since the unit desired for each pigment of each sample was µg/cell and not µg/mL, the values of equations mentioned above were divided by the number of cells of each sample.

2.3. Quantification of proteins

The white insolubilized pellet from pigment extraction was afterwards treated with solutions for the quantification of proteins following the Lowry method (Waterborg & Matthews, 1994).

Standard trend line for protein quantification was obtained by analysing fourteen samples with a known Bovine Serum Albumin (BSA) final concentration. The concentration of the stock solution was 1 mg/mL. SDS solution and BSA stock solution were added to sterile Eppendorf tubes according to the following table:

Table 5. A list of BSA concentrations for the standard trend line.

BSA final (µg)	***SDS solution (µL)***	***BSA stock* 1 mg/mL *(µL)***
0	500	0
5	495	5
10	490	10
20	480	20
30	470	30
40	460	40
50	450	50
60	440	60
70	430	70
80	420	80
90	410	90
100	400	100
115	385	115
125	375	125

Firstly, 500 µL of SDS working solution, that contained 0,1 SDS 10%, 0,125 NaOH 0,8M and 0,775 H_2O, were added to both the algal samples.

Secondly, 500 µL of Reagent A, prepared daily by mixing ¼ H_2O, ¼ NaOH 0,8M, ¼ Copper-Tartrate-Carbonate solution and ¼ SDS 10%, were added both to algal samples and standard samples. These had to be vortexed quickly and incubated in the dark for 10 minutes.

Thirdly, 250 µL of Reagent B, containing ⅕ Folin & Ciocalteu's Phenol Reagent and ⅘ H_2O, were added to the algal and standard samples which were quickly vortexed and placed in the dark for another 30 minutes. The folin phenol reagent bound to the proteins within samples, which was possible to observe through the viration of colour from transparent to blue (Figure 7).

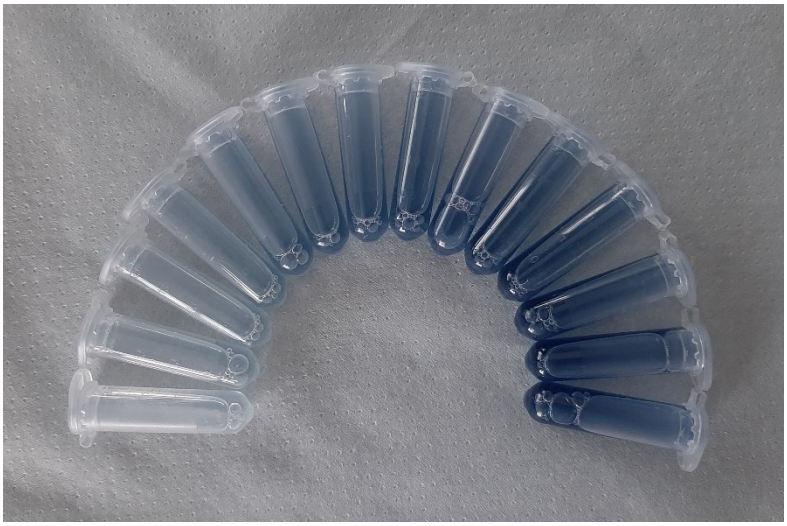

Figure 7. Viration of colour from transparent to blue, from lower to higher concentrations of BSA solution, respectively.

After the time has passed, algal samples and trend line samples were ready to be analysed with a spectrophotometer.

The spectrophotometer ONDA UV-31 was used to quantify the concentration of proteins within the analysed samples. It was necessary to switch on the visible lamp of the analyser and let it heat up 10 minutes prior to the analysis. A fixed wavelength (λ) of 750 nm was set as referred in Lowry, 1951. Approximately 15 minutes afterwards, the blank was exhibited with 700 µL distilled water that was pipetted in a quartz cuvette (Precision cell made of Quartz SUPRASIL by Hellma ®, with light path

10 mm). Once the spectrophotometer did the blank, it was time to analyse the samples for the standard trend line. The same volume of samples with increasing concentrations of BSA solution were read one after the other. Between each sample, the cuvette was rinsed with distilled water three times. The same process was applied to the samples taken from algal cultures. Each resulting absorbance was carefully annotated in the laboratory notebook. Having finished with analysis, the visible lamp was switched off, as well as the spectrophotometer itself, and the cuvette was cleaned and let dry.

The obtained data was inserted in Microsoft Office Excel (.xlsx) program and furtherly processed. To begin with, it was necessary to insert a scatter plot relative to the wavelengths measured from the BSA solution samples. The trend line and its equation were calculated by the software (Figure 8).

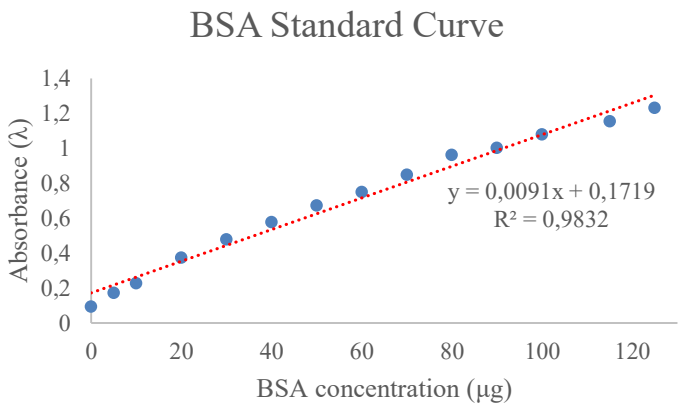

Figure 8. BSA standard curve with the trend line and its equation. Absorbance is measured in respect to the known concentrations of BSA solution.

The following equation was obtained:

$y = k \cdot x + m$; where y is the wavelength; k is the slope; x is the concentration of proteins found in the samples; and m is the intersection of the y axis.

In order to determine the concentration of proteins within samples from algal cultures, the above mentioned equation was adjusted as it follows:

$x = \frac{y-m}{k}$; where m and k values were given by the trend line equation and y was represented by the measured absorbance of each sample. By using this adjusted equation, it was possible to calculate the concentration of proteins of each sample from algal cultures.

2.4. Fourier Transform Infrared Spectroscopy Analysis

The organic composition of *Tetraselmis suecica*, *Dunaliella salina* and *Phaeodactylum tricornutum* cells was measured with Fourier transform infrared (FT-IR) spectroscopy.

The Fourier Transform Infrared Spectroscopy has developed into a quick and relatively easy tool for the analysis of macromolecular pools in individual cells among microscopic organisms, such as bacteria, fungi and algae (Ubbink & Scha, 2003; Bo et al., 2010; Dilek (Yalcin) Duygu, 2012). Through this analysis, it is possible to assess the vibrationally active functional groups of macromolecules like carbohydrates, proteins and lipids, and so depict the cell composition of marine microalgae (Giordano et al., 2001; Hirschmugl et al., 2006; Giordano et al., 2009; Jebsen et al., 2012). Cells were prepared as described in Domenighini & Giordano, 2009, as detailed below.

Collected microalgal cells (5 mL of exponential phase culture) were washed 3 times with the ammonium formate 0.5M. The solution is iso-osmotic to the culture medium AMCONA. Cells were finally resuspended in 150 µL ammonium formate.

A quantity of 50 µL was used for each strumental replica, deposited on FTIR sample discs and dried at 80°C overnight. In parallel, the blank was prepared by using 50 µL ammonium formate. The acquisition of organic composition of each sample was obtained with the Bruker Tensor 27 IR © spectrophotometer. The sample disks dried overnight at 80°C were placed into Bruker tensor sample holder. Parameters for analysis were set in the OPUS 6.0 Software before starting the acquisition.

Blank spectrum was recorded at first, between 4000 cm^{-1} and 400 cm^{-1}, at a spectral resolution of 4 cm^{-1}, followed by sample analyses. The abovementioned range of absorptions was selected because

it serves well for the semi-quantification of carbohydrates, proteins and lipids. Table 6 indicates which peaks represent the absorptions of macromolecules for the scope of this study.

In the following step, the acquired data was analysed by fitting the obtained curves between 1800 cm^{-1} and 900 cm^{-1}.

Table 6. Spectral absorption peaks for the semi-quantification of organic macromolecules by using the Fourier Transform Infrared Spectroscopy.

Macromolecule	***Absorption spectra (cm^{-1})***	***Band assignment***	***Comments***
Carbohydrates	900 - 1200±10	C-O-C of etheric groups of carbohydrates	Primarily due to carbohydrates, peak at 1155 cm is used as a proxy for semi-quantification of carbohydrates.
Proteins	1650±10	C=O of amides associated with proteins	Amide I band used as a proxy for proteins.
Lipids	1740±5	C=O of ester functional groups	Triglycerides used as a proxy for semi-quantification of lipids.

2.5. Carbon and nitrogen quantification

Tetraselmis suecica, *Dunaliella salina* and *Phaeodactylum tricornutum*, samples elemental composition of carbon and nitrogen were measured. There is a rather important stoichiometric relation between carbohydrate, protein and lipid composition and organic CHN contents (Gnaiger et al., 2012). The analysis was done with an Elemental Combustion System (ECS4010, Costech Analytical Technologies Inc., Milano, Italy) that allows an accurate and precise elemental quantification.

Different volumes were transferred from each Erlenmeyer flask containing microalgal cultures in exponential growth phase to sterile Falcon tubes under the biological safety cabinet. Samples were

centrifuged at 4500 *g* for 10 minutes. Following the removal of the surnatant, they were washed with ammonium formate 0.5M solution two times to eliminate salts. Finally, the pellets were transferred into 2 mL Eppendorf tubes with 1 mL ammonium formate 0,5M, centrifuged at 10000 *g* for 10 minutes, and the surnatant was thrown away. Eppendorf tubes containing washed pellets where then weighted and placed in the oven at 80°C till stable dry weight was reached.

While the CHN Analyser was being prepared to run, samples were processed. First of all, it was necessary to prepare approximately 12 aluminium capsules containing a known weight in the range of 0,1 – 1,2 mg of sulphanilamide, an organic compound. In addition, a small quantity of vanadium had to be added. Each of these 12 capsules served as standards for the calibration of the CHN Analyser (Figure 9).

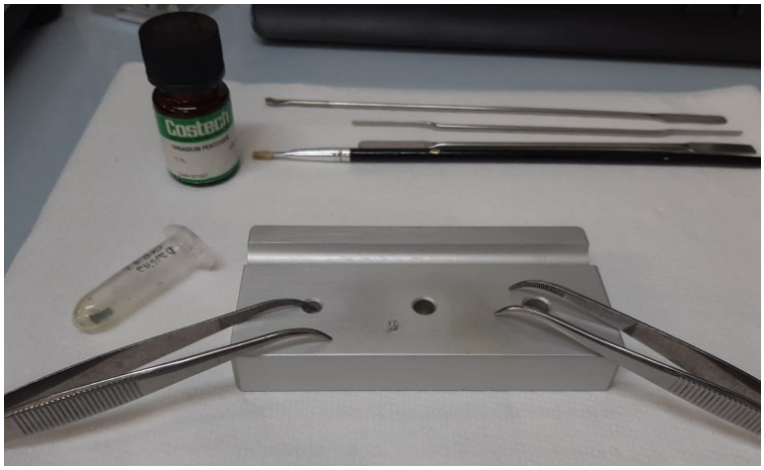

Figure 9. Preparation of aluminium capsules for the elemental analysis using a CHN Analyser.

Two capsules for each sample were carefully weighted, a small amount (0,3 mg - 1,1 mg) was placed in and a small quantity of vanadium was added. Each capsule had to be closed strategically with tweezers, in order to remove any spaces filled with air. Lastly, two strumental replicas were ran through the CHN Analyser. Capsules had to pass in a column in which they were burned at 900°C and the gasses produced during perfect combustion were detected by the instrument.

Elemental composition, in terms of carbon, hydrogen and nitrogen, was determined for each cell of each microalgal species and regime.

2.6. *In vivo* chlorophyll fluorescence measurements

Throughout the last few decades, chlorophyll *a* fluorescence measurements have allowed in depth studies in the fields of plant physiology (Krause & Weis, 1984). In the introductive section on Light reactions, it was discussed that the light energy is absorbed by chlorophyll molecules for photosynthesis. Nonetheless, under conditions of light stress, photosynthetic organisms avoid photoinhibition through the dissipation of non-photochemical quenching (NPQ), else known as heat. In order to evaluate photochemistry and photoprotection by excess energy dissipation within the microalgal species *Tetraselmis suecica*, *Dunaliella salina* and *Phaeodactylum tricornutum* acclimated to different light regimes, *in vivo* measurements of the photosystem II were performed using a Dual-PAM-100 measuring system (Heinz Walz GmbH, Effeltrich, Germany).

Algal cells were collected by centrifugation at 4500 *g* for 10 min in order to obtain:

- 6×10^6 cells/2 mL for *Tetraselmis suecica*;
- 6×10^6 cells/2 mL for *Dunaliella salina*;
- 20×10^6 cells/2 mL for *Phaeodactylum tricornutum*;

according to the internal laboratory protocol. After centrifugation, the cells were kept in the dark for 30 minutes to allow full oxidation of the photosynthetic electron transport chain. The analysis of the fluorescence kinetics was recorded *in vivo* with the DUAL-PAM-100 measuring system was switched on and the parameters were set accordingly.

The competitiveness between these decaying processes takes place and this can be seen in changes of the emitted fluorescence (Bolhàr-Nordenkampf & Öquist, 1993; Krause & Weis, 1984).

The measuring light (FML) was utilised to monitor fluorescence through weakly pulsing light, that does not activate the electron transport chain. Its intensity was kept the same in all samples, and it

was equal to 24 $\mu mol \cdot m^2 \cdot s^{-1}$. On the other hand, actinic light (AL) was employed to induce photosynthesis, and therefore, the electron transfer. It was equivalent to 126 $\mu mol \cdot m^2 \cdot s^{-1}$. The intensity of six for saturation pulse (SP), which consists in fast light pulsing, was implemented in order to eliminate any quenching due to photochemistry (qP) and quantify only the non-photochemical quenching (Baker, 2008).

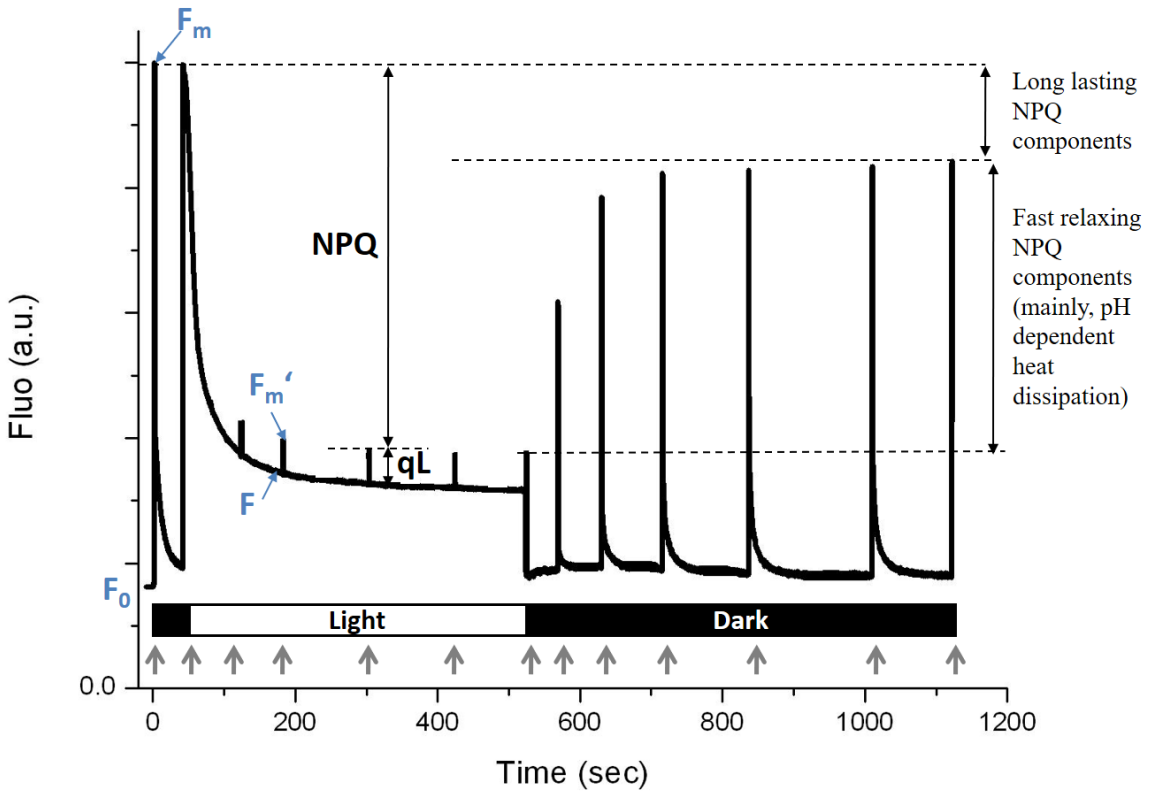

Figure 10. Schematic representation of the chlorophyll (Chl) induction kinetics. The measuring light is activated throughout the whole analysis and the actinic light (AL) is switched on only for a short time at the beginning. The grey arrows indicate the application of a short pulse of saturating light. F, F_0, F_m and F_m' parameters are indicated. Long-lasting and short-lasting (i.e. pH-dependent heat dissipation) NPQ components are detected in the ranges indicated. Modified from Müller et al., 2001.

Several parameters can be obtained from *in vivo* Chlorophyll fluorescence analyses (Figure 10). The maximum quantum yield of photochemistry by PSII, F_v/F_m, is given after acclimation to darkness and it is calculated with the following equation:

$F_v/F_m = (F_m - F_0)/F_m$;

where F_m is the maximal fluorescence yield, reached during a saturation pulse (SP), and F_0 is the value at which all the PSII reaction centres are open (Heinz Walz & Walz, 2006).

The quantum yield of the PSII, Y(II), is determined according to Baker, 1989 as:

$Y(\mathrm{II}) = (F'_m - F)/F'_m$

The Y(II) varies between 0 and 1. For instance, when it is equal to 0,5, it means that one half of the absorbed quanta undergo photochemical charge separation at PSII reaction centres, thus being converted into chemically fixed energy, whereas the other half is dissipated under the forms of heat and fluorescence.

The fraction of open PSII centres is determined by the coefficient of photochemical quenching, qP, that can give values between 0 and 1, all PSII centres closed or opened, respectively. This coefficient is calculated as follows:

$qP = \frac{F'_m - F}{F'_m - F'_0}$;

where F_m' is the maximum fluorescence and F_0' is the minimum fluorescence under reduced plastoquinone pool conditions (Ogawa et al., 2017). The qP parameter is based on the "puddle model" of PSII.

The fraction of open PSII centres based on a "lake model" is defined by the coefficient of photochemical quenching, qL, and can be calculated as:

$$qL = \frac{F'_m - F}{F'_m - F'_0} \times F'_0/F = qP \times F'_0/F$$

Non-photochemical quenching (NPQ) is calculated from:

$$NPQ = \left(\frac{F_m}{F'_m}\right) - 1$$

With this parameter, it is possible to monitor the apparent rate constant for heat loss from PSII (i.e. pH-dependent heat dissipation).

The abovementioned parameters were investigated through the analysis of dark acclimated cells.

2.7. Statistical analyses

All experiments were done at least in triplicate (three different batch cultures), for each species and light condition. All results were expressed as mean ± standard deviation. The statistical significance of the data of the maximum growth rate (μ_{max}), maximum quantum yield of photochemistry by PSII (F_v/F_m), chlorophyll content, Chl *a*/Chl *b* (for *T. suecica* and *D. salina*) and Chl *a*/Chl *c* (for *P. tricornutum*), elemental composition, quantification of proteins, macromolecular FTIR ratios and the carbohydrates and lipids semiquantification, was tested by a one-way ANOVA with Tukey-Kramer post-hoc test, except for the elemental composition where no post-hoc test was applied.

The level of significance was set to 95%, thus values of p lower than 0.05 were considered statistically significant.

RESULTS

3.1. Growth

Batch cultures of *Tetraselmis suecica, Dunaliella salina* and *Phaeodactylum tricornutum* grown in continuous control light intensity (CTR), low light (LL) or with day/night cycles (PP) (see section 2.1 in MATERIALS AND METHODS for detail on growth conditions) were monitored daily by cell counts.

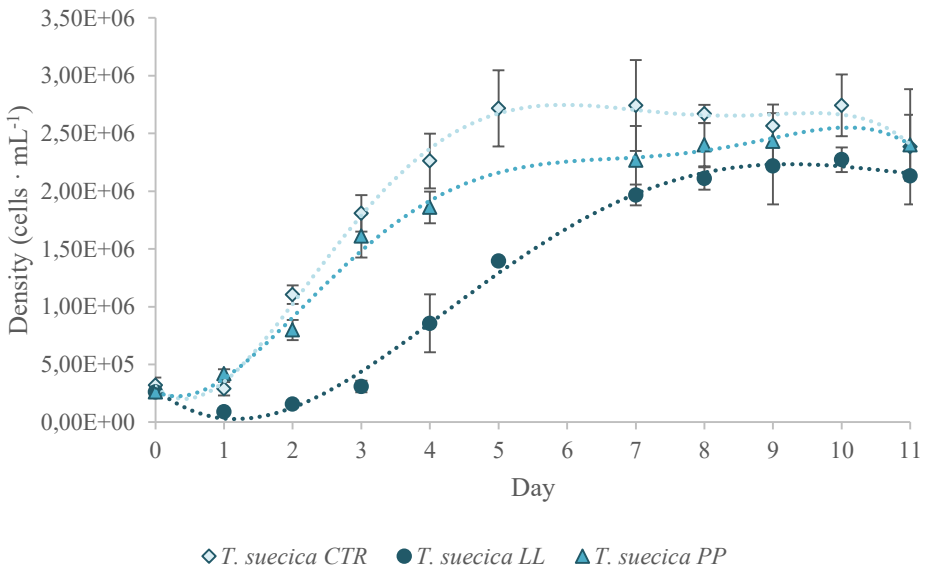

Figure 11. Eleven days' growth curves from batch cultures of *Tetraselmis suecica*. In light blue are represented cells under control conditions (CTR). In dark blue are *T. suecica* cells under low light conditions (LL). The intense blue curve indicates cells under photoperiod (PP). Counts were performed on the indicated days. Data are presented as mean ± standard deviations (n=3).

T. suecica CTR cells showed a 1-day lag phase, then grew exponentially till day 5 when they reached the steady growth phase, with a cell density of about 2.7 million cells·mL^{-1} (Figure 11). Under LL conditions, cells had a longer lag phase, exponential growth started on day 3 and lasted till day 9

when steady state was reached, with final cell yield of about 2.3 millions of cells·mL^{-1}. Those cells that were acclimated to PP conditions started the exponential phase on day 1 and reached the stationary growth with 2.4 millions of cells·mL^{-1} on day nine.

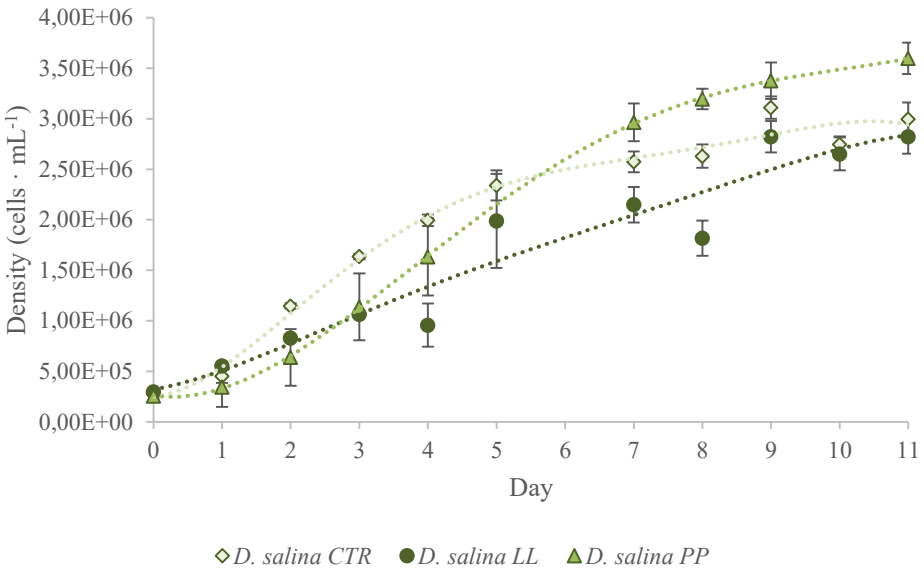

Figure 12. Eleven days' growth curves from batch cultures of *Dunaliella salina*. In light green are represented cells under control conditions (CTR). In dark green are *D. salina* cells under low light conditions (LL). The intense green curve indicates cells under photoperiod (PP). Counts were performed on the indicated days. Data are presented as mean ± standard deviations (n=3).

Under CTR conditions, *D. salina* started growing exponentially from day one and entered the steady phase on the ninth day, having reached a density of about 3 millions of cells·mL^{-1} (Figure 12). In LL conditions, cells number increased already from the inoculation to day 1, exponential growth was slower than CTR but the final cell density was similar to that of the CTR and equal to about $2.8 \cdot 10^6$ cells·mL^{-1}. As for the cells under PP conditions, exponential growth started at day 1, with the stationary phase being reached on day 10 with about $3.6 \cdot 10^6$ cells·mL^{-1}, the highest cell concentration among the conditions tested in this thesis.

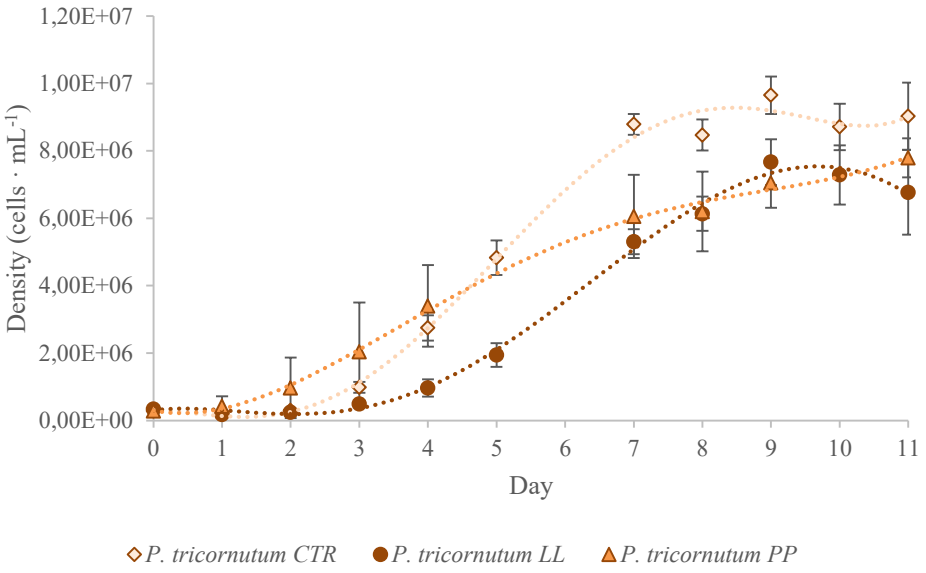

Figure 13. Eleven days' growth curves from batch cultures of *Phaeodactylum tricornutum*. In light orange are represented cells under control conditions (CTR). In brown are *P. tricornutum* cells under low light conditions (LL). The intense orange curve indicates cells under photoperiod (PP). Counts were performed on the indicated days. Data are presented as mean ± standard deviations (n=3).

In Figure 13, the growth curves of *Phaeodactylum tricornutum* cells are show. CTR cells exhibited a lag phase till day 3, when they started growing exponentially and entered into a steady state growth on the day seven (8.8 millions of cells per mL). Under LL, *P. tricornutum* remained in the lag phase between day zero and three. It started growing exponentially from day four but its growth was lower and longer than in CTR. Moreover, the steady state was reached on day nine, when cells grew to approximately 7.7 million cells·mL^{-1}. Even if an initial lag phase was observed in the mentioned regimes, it was not the case of cells acclimated to PP conditions. In fact, the cells had grown exponentially already from day one. No stationary growth phase has been observed after day eleven, when there were $7.8 \cdot 10^6$ cells·mL^{-1}.

3.1.1. Maximum growth rate

The cultures maximum growth rates were determined on the exponential phase of the curves presented in Figure 11,Figure 12 andFigure 13. As shown in Figure 14, *T. suecica* had a higher maximum growth rate, μ_{max}=0.92, under CTR, than the LL and PP conditions, where it was on average 0.84 and 0.56, respectively. The green algae *D. salina* grew maximally under CTR conditions (μ_{max}=0.71). In LL, the maximum growth rate was 30% lower than in CTR, while μ_{max} in PP was 15% lower compared to the CTR. The diatom *P. tricornutum* had the highest growth rate in CTR conditions (μ_{max}=1.10), as well as among the species, whereas in LL it was lower (μ_{max}=0.68). Under PP, the maximum growth rate of *P tricornutum* was lower than in CTR but higher than in LL (μ_{max}=0.82).

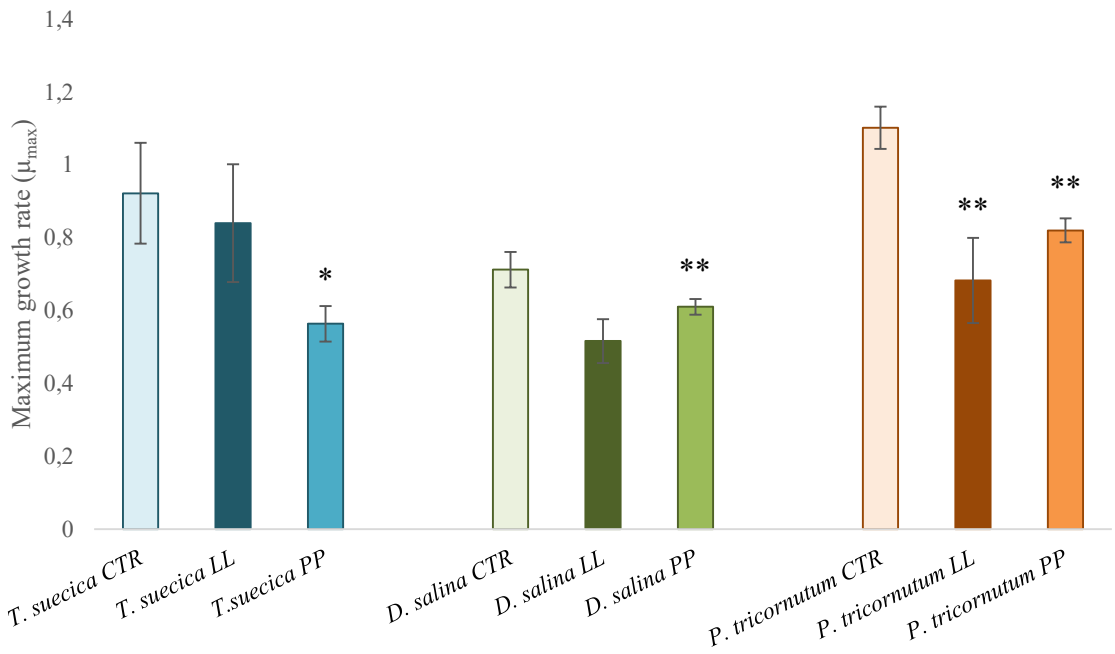

Figure 14. Maximum growth rates (μ_{max}) of *T. suecica* (shades of blue), *D. salina* (shades of green) and *P. tricornutum* (shades of orange) under different light regimes. The left column of each microalgae represents the control conditions (CTR). The middle column shows the low light regime (LL). The right column indicates a photoperiod (PP). Data are presented as mean ± standard deviations (n=3). The statistical significance of the data was tested by a one-way ANOVA

with Tukey-Kramer post-hoc test. Asterisks represent the statistical significance of the average maximum growth rate (μ_{max}) in LL and PP conditions with respect to that of CTR conditions (* = $p < 0.05$; ** = $p < 0.01$; *** = $p < 0.001$).

3.2. Characterization of microalgal Photosynthesis

Maximum PSII quantum yield (F_v/F_m), photochemistry and activation of photoprotection mechanisms upon exposure to increasing illumination ("light curve" experiments, see section 2.6 in MATERIALS AND METHODS for details) were evaluated *in vivo* on cells of the three algal species under investigation, grown in the different light conditions and analysed during the mid-exponential phase.

3.2.1. Photosynthetic efficiency

Maximum PSII quantum yield (F_v/F_m) values after a 30 minute dark acclimation of cells is presented in Figure 15. The maximum photosynthetic efficiency (F_v/F_m) in *T. suecica* CTR showed was about 0.41, the lowest value obtained in our experiments, both among the different regimes and different algal species. In LL and PP, F_v/F_m was about 0.69 and 0.71, respectively. The maximum quantum yield of photochemistry by PSII in *D. salina* was poor in CTR, and equaled to 0.48. Under LL conditions, *D. salina* performed photosynthesis with an almost 20% higher efficiency (F_v/F_m=0.63). However, it was the greatest when cells were acclimated to the PP, when it reached an F_v/F_m of 0.70. *P. tricornutum* CTR had a photosynthetic efficiency of about 0.48. Under LL and PP, it showed a similar maximum quantum yield of PSII, which was 0.72 in LL and 0.69 in PP. In all species, the maximum quantum yield of PSII was significantly greater in LL and PP conditions with respect to the CTR.

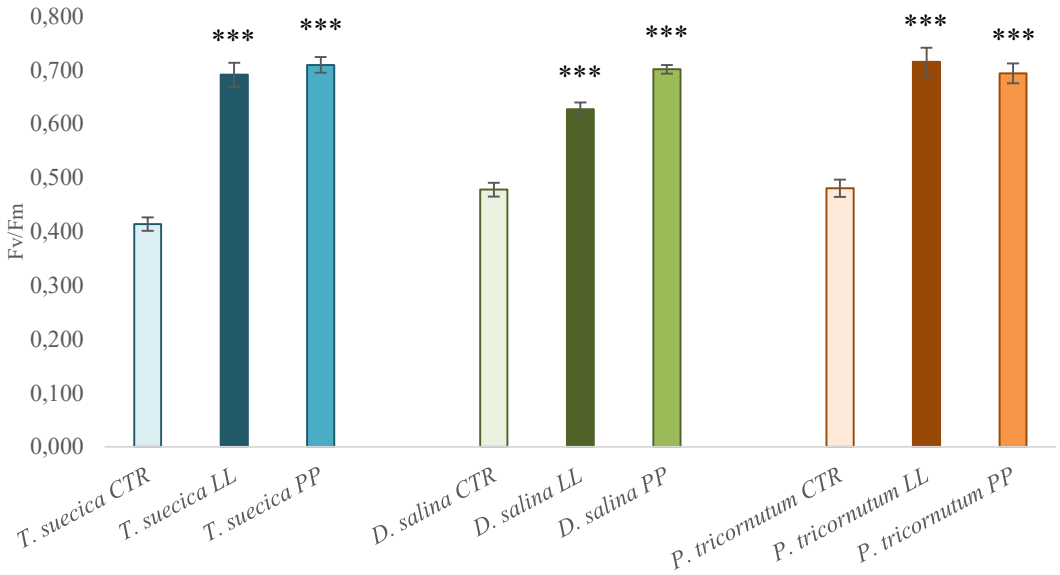

Figure 15. Maximum quantum yield of photochemistry by PSII (F_v/F_m) of *T. suecica* (shades of blue), *D. salina* (shades of green) and *P. tricornutum* (shades of orange) under different light regimes. Data are presented as mean ± standard deviations (n=4). The statistical significance of the data was tested by a one-way ANOVA with Tukey-Kramer post-hoc test. Asterisks represent the statistical significance of the F_v/F_m in LL and PP conditions with respect to that of CTR conditions (* = $p < 0.05$; ** = $p < 0.01$; *** = $p < 0.001$).

3.2.2. Photosynthetic kinetics from light curves

3.2.2.1. Quantum yield of photochemical energy conversion in PSII

The same samples used for F_v/F_m estimation have also been analysed with "light curves" kinetics, where, after 30-minute dark acclimation, cells were exposed to subsequent steps of illumination, starting from very low light intensity to about 2000 $\mu mol \cdot m^2 \cdot s^{-1}$, to evaluate how photosynthesis and photoprotection were activated by the different samples in response to variable illumination.

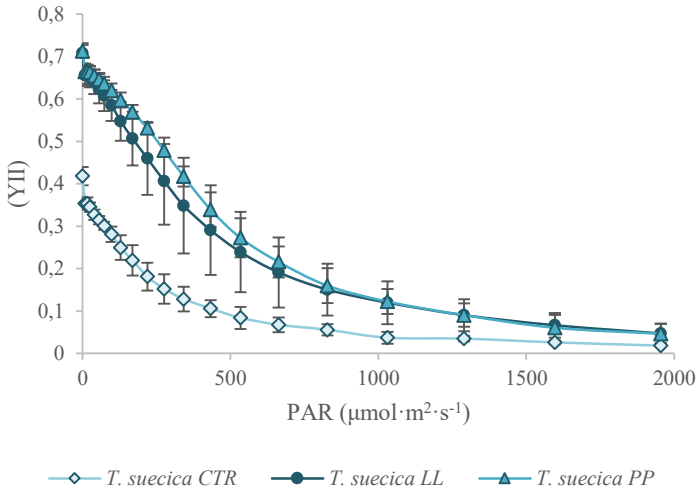

Figure 16. Quantum yield of photochemical energy conversion in PSII, or Y(II), of *Tetraselmis suecica* under different light regimes: CTR, LL and PP). Data are presented as mean ± standard deviations (n=4 for CTR and PP, n=5 for LL).

At low actinic lights, the PSII quantum yield (Figure 16) in *T. suecica* cells under CTR was almost half of that of the other two conditions, following the lower F_v/F_m of CTR. The amount of energy absorbed and used for photochemistry, Y(II), decreased progressively with the increasing PAR in cells from all tested growth light conditions, CTR, LL and PP, although the former was characterized by lower Y(II) values with respect to LL and PP for most of the light curve kinetics.

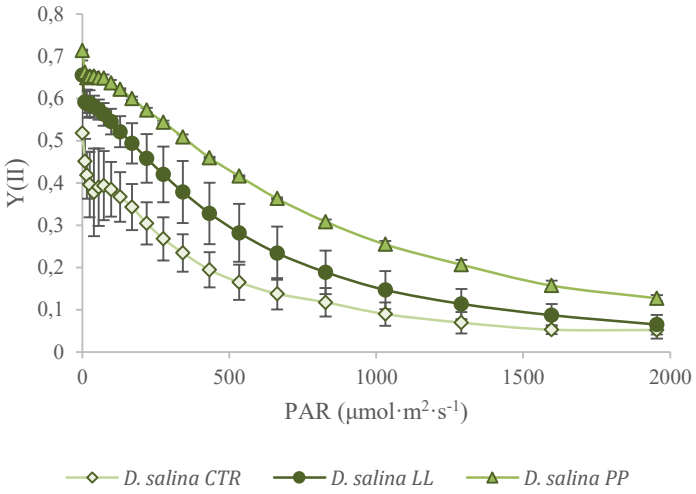

Figure 17. Quantum yield of photochemical energy conversion in PSII, or Y(II), in *Dunaliella salina* under different light regimes: CTR, LL and PP. Data are presented as mean ± standard deviations (n=6 for CTR, n=8 for LL, n=4 for PP).

As observed in Figure 17, *D. salina* showed results similar to *T. suecica* above, with the CTR sample showing the lowest Y(II) values at low PAR, and all samples decreasing Y(II) as the PAR increased. However, *D. salina* CTR cells Y(II) showed a peculiar kinetic visible at low PAR. The Y(II) in control decreased rapidly, increased slightly at around 70 µmol·m^2·s^{-1}, to then decrease again. PP samples also followed a similar pattern of that observed in CTR, but the initial peak was observed to be decreasing from around 100 µmol·m^2·s^{-1} on.

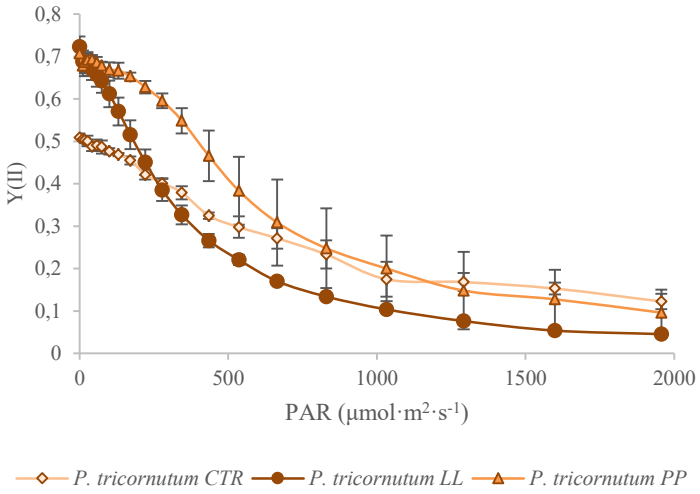

Figure 18. Quantum yield of photochemical energy conversion in PSII, or Y(II), in *Phaeodactylum tricornutum* under different light regimes: CTR, LL and PP. Data are presented as mean ± standard deviations (n=6 for CTR and LL, n=4 for PP).

The quantum yield of photochemistry for PSII (Figure 18) was the lowest in *Phaeodactylum tricornutum* cells of CTR and decreased almost linearly throughout the analysis. Even though the Y(II) was the highest in cells acclimated to LL, it decreased exponentially and at the end displayed the lowest value among all conditions. As for the *P. tricornutum* under PP, the quantum yield of photochemistry for PSII decreased slowly at the beginning, whereas from approximately 300 $\mu mol \cdot m^2 \cdot s^{-1}$ on, it decreased exponentially and was slightly lower than in CTR.

3.2.2.2. *Fraction of opened PSII centres*

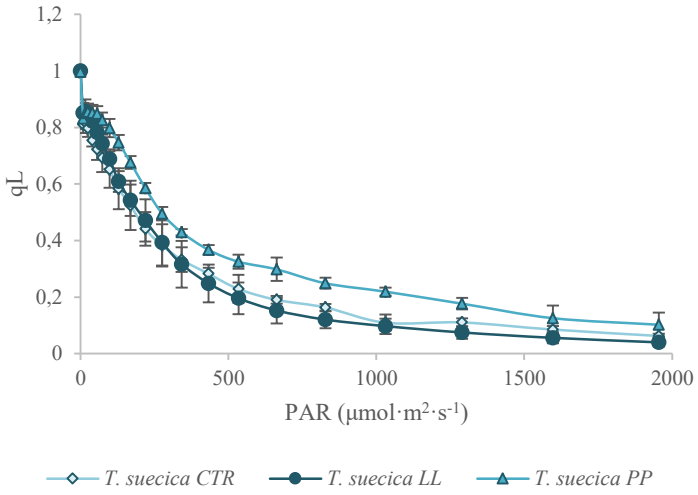

Figure 19. Fraction of PSII centres that are 'open,' or qL, of *Tetraselmis suecica* under different light regimes: CTR, LL and PP. Data are presented as mean ± standard deviations (n=4 for CTR and PP, n=5 for LL).

The fraction of PSII centres that are 'open' (with Q_A oxidized) is designated with the parameter qL. From Figure 19, the qL was akin in both CTR and LL conditions of *T. suecica*. Similarly to the parameter Y(II) above, the qL values within each sample also decreased upon increase of PAR irradiance. Cells acclimated to PP followed a similar pathway, but the value of qL was the highest among all conditions.

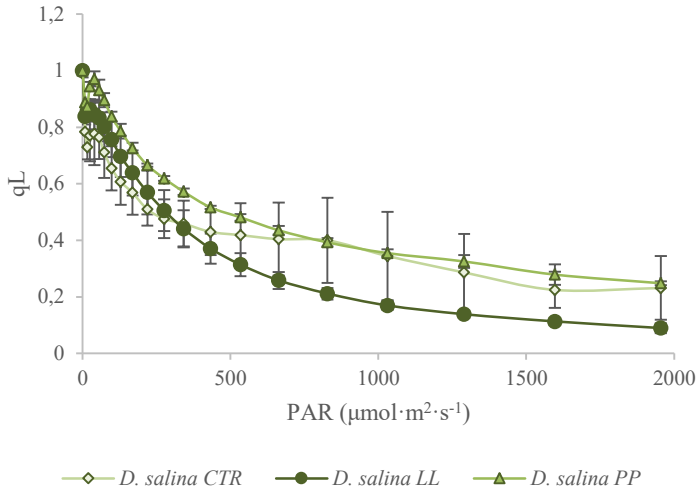

Figure 20. Fraction of the PSII centres that are 'open' (qL) in *Dunaliella salina* under different light regimes: CTR, LL and PP. Data are presented as mean ± standard deviations (n=6 for CTR, n=8 for LL, n=4 for PP).

In Figure 20, the qL decreased substantially at the beginning of analysis in *D. salina* cells of CTR, then followed by a slight increase at a light intensity of 50 µmol·m^2·s^{-1}, to then decrease as a response to increasing PAR. Under LL, *D. salina* was alike with CTR. The initial values of qL were, however, higher in LL acclimated cells. In addition, the value decreased more than in CTR, with the last qL value being the lowest among all conditions. In cells of *D. salina* acclimated to PP, the qL parameter followed the same pattern as in LL, with the only difference of being higher than in other two conditions.

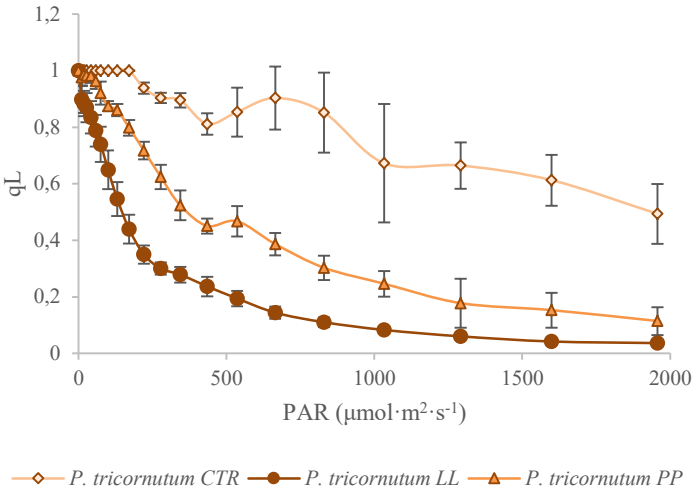

Figure 21. Fraction of the PSII centres that are 'open' (qL) in *Phaeodactylum tricornutum* under different light regimes: CTR, LL and PP. Data are presented as mean ± standard deviations (n=6 for CTR and LL, n=4 for PP).

As seen in Figure 21, the fraction of the opened PSII centres (qL) was the highest in CTR of *Phaeodactylum tricornutum*. After a slight decrease, the cells exhibited an increase-decrease pattern between 500 and 1000 µmol·m^{2}·s^{-1}, and again decreased afterwards. The qL under LL decreased exponentially and was the lowest of all conditions through the analysis. Under PP conditions, the values decreased almost exponentially, except when they showed a small peak at around 500 µmol·m^{2}·s^{-1}.

3.2.2.3. Non-photochemical quenching

The light curve experiments also allowed to obtain non-photochemical quenching (NPQ) kinetics. This parameter mostly estimates how much energy is dissipated as heat from PSII, but other regulatory mecchanisms, like state transitions (i.e. the phosphorylation of LHCII proteins which detach from PSII) can also contribute to the NPQ value.

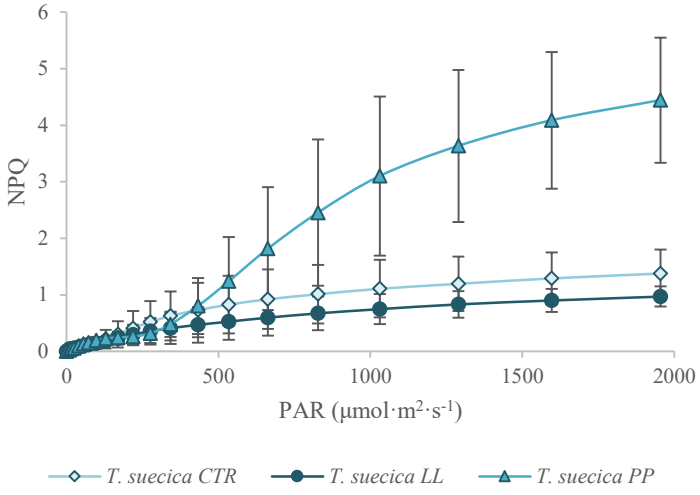

Figure 22. Non-photochemical quenching (NPQ) of *Tetraselmis suecica* under different light regimes: CTR, LL and PP. Data are presented as mean ± standard deviations (n=4 for CTR and PP, n=5 for LL).

Non-photochemical quenching (Figure 22) in cells of *T. suecica* under CTR conditions was induced steadily. The pattern appeared nearly similar in *T. suecica* under LL conditions throughout the whole analysis, but the NPQ values were lower. In the case of *T. suecica* acclimated to PP, NPQ seemed to be low within the increasing PAR up to 342 µmol·m^{2}·s^{-1}, but was then induced to 4-fold higher than in CTR.

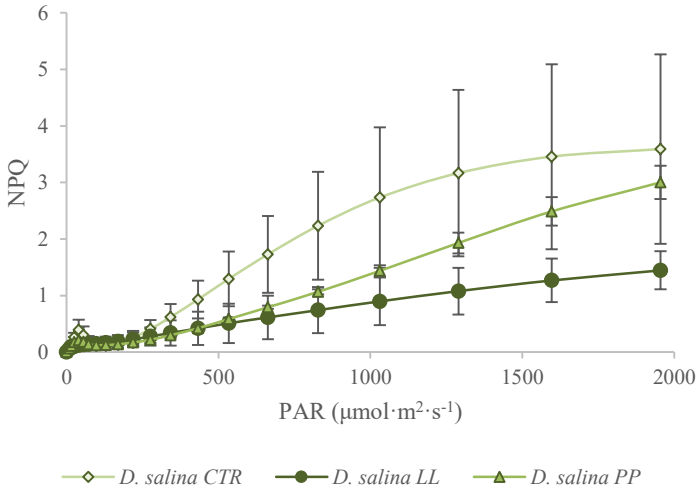

Figure 23. Non-photochemical quenching (NPQ) in *Dunaliella salina* under different light regimes: CTR, LL and PP. Data are presented as mean ± standard deviations (n=6 for CTR, n=8 for LL, n=4 for PP).

In Figure 23, the non-photochemical quenching in *D. salina* in CTR conditions reached a small first peak at 40 µmol·m^2·s^{-1} on, which then relaxed and started to increase again from around 130 µmol·m^2·s^{-1}. The saturation point was reached at around 1600 µmol·m^2·s^{-1}. Under LL conditions, *D. salina* did not show the initial peak at 40 µmol·m^2·s^{-1} as observed in CTR. NPQ underwent an almost linear induction throughout the analysis but it was substantially lower than in other conditions. In *D. salina* acclimated to PP, the NPQ initial peak at 40 µmol·m^2·s^{-1} was observed but it was half as high as in CTR conditions. Afterwards, the peak relaxed following a similar pattern than in CTR, to then increase linearly with the increasing PAR. This induction in NPQ was higher than in *D. salina* acclimated to LL. Additionally, it did not reach the saturation point at the end of analysis.

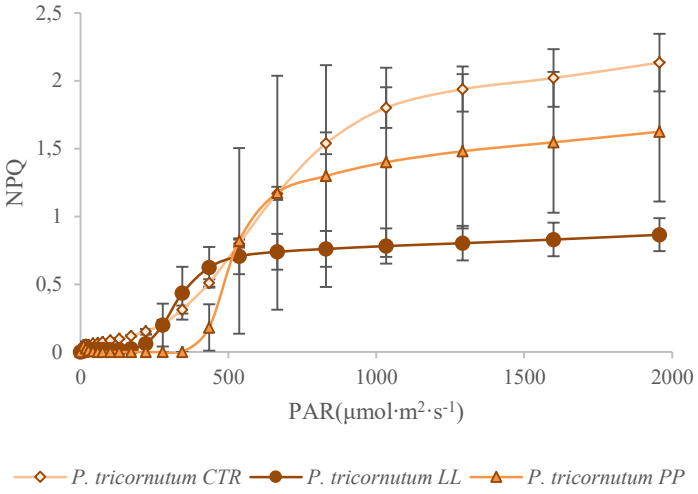

Figure 24. Non-photochemical quenching (NPQ) in *Phaeodactylum tricornutum* under different light regimes: CTR, LL and PP. Data are presented as mean ± standard deviations (n=6 for CTR and LL, n=4 for PP).

In all samples of *Phaeodactylum tricornutum*, NPQ was very low at the beginning, then increased rapidly reaching maximal value in few light steps. Yet, the specific light intensities which activate NPQ and final values reached were different in CTR, LL and PP samples. In CTR and LL, NPQ was

low until around 300 µmol·m^2·s^{-1}, while PP activated NPQ at almost 500 µmol·m^2·s^{-1} (Figure 24). LL cells displayed the lowest final NPQ, that reached saturation at about 500 µmol·m^2·s^{-1}. CTR final NPQ was almost twice than that of LL. When cells were acclimated to PP, the values were almost zero up to 400 µmol·m^2·s^{-1} and then increased exponentially to the saturation point seen from approximately 600 µmol·m^2·s^{-1}.

3.2.2.4. Q_A reduction

Fluorescence analyses in light curve kinetics also allow to infer the relative reduction of Q_A, used as a proxy for the reduction of the whole photosynthetic electron transport chain.

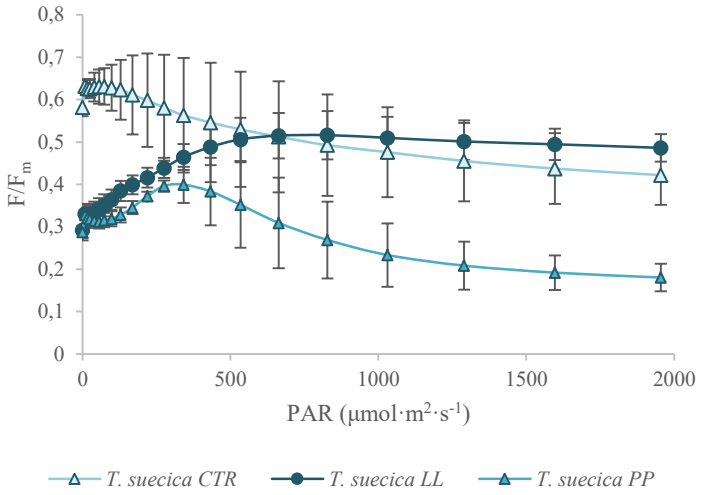

Figure 25. Level of fluorescence when Q_A is relatively reduced (F/F_m) of *Tetraselmis suecica* under different light regimes: CTR, LL and PP. Data are presented as mean ± standard deviations (n=4 for CTR and PP, n=5 for LL).

As seen in Figure 25, at the beginning, the Q_A relative reduction values (F/F_m) were the highest in *T. suecica* under CTR conditions and decreased afterwards. Instead, the fluorescence levels in *T. suecica* LL were half of the CTR at low PAR, to then increase as PAR increased, with values similar to CTR from about 600 PAR. Cells acclimated to PP, exhibited a similar trend as in control

conditions, except that the fluorescence levels were 2-fold lower and the increase-decrease pattern occurred in the first quarter of analysis.

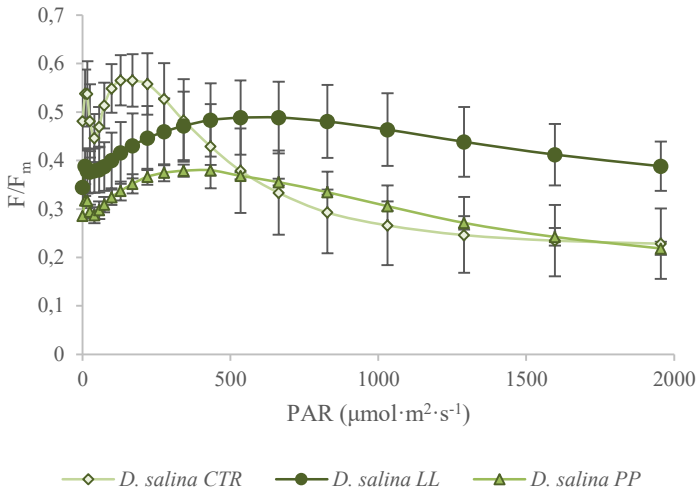

Figure 26. Level of fluorescence when Q_A is relatively reduced (F/F_m) in *Dunaliella salina* under different light regimes: CTR, LL and PP. Data are presented as mean ± standard deviations (n=6 for CTR, n=8 for LL, n=4 for PP).

As shown in Figure 26, *D. salina* in CTR conditions showed a peculiar kinetic. Values first decreased, then, F/F_m peak at 200 µmol·m^2·s^{-1} to decrease afterwards. Cells of *D. salina* acclimated to LL also showed an undulating patter as in CTR, except that the peak was less pronounced and observed at approximately 650 µmol·m^2·s^{-1}, and then the F/F_m decreased, but much less then in CTR. PP F/F_m values kinetic was similar to LL but characterized by lower values throughout the analyses.

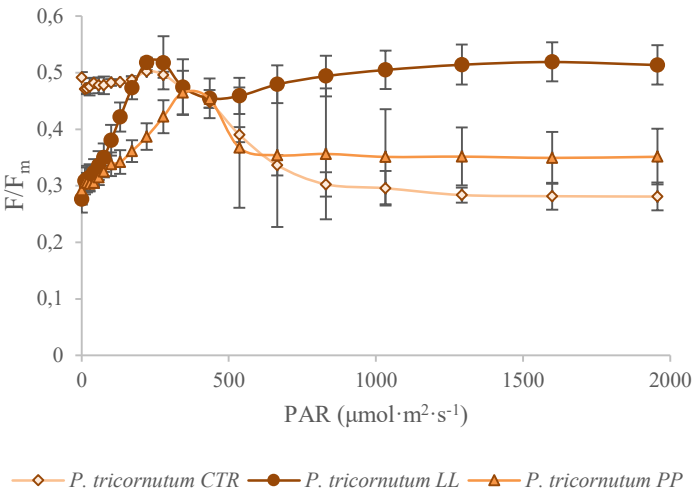

Figure 27. Level of fluorescence when Q_A is relatively reduced (F/F_m) in *Phaeodactylum tricornutum* under different light regimes: CTR, LL and PP. Data are presented as mean ± standard deviations (n=6 for CTR and LL, n=4 for PP).

As cells of *Phaeodactylum tricornutum* (Figure 27) under CTR were illuminated, the F/F_m was the highest in respect to the other conditions. From about 400 µmol·m^2·s^{-1}, F/F_m values decreased and again reached a plateau from 800 µmol·m^2·s^{-1} on. In LL samples, cells increased the fluorescence to a peak at approximately 350 µmol·m^2·s^{-1}, which was then kept roughly stable and higher than both CTR and PP samples. Cells acclimated to PP exhibited a kinetic similar to LL, but were characterized by lower values.

3.2.3. Chlorophyll content

The chlorophyll content was determined in *Tetraselmis suecica, Dunaliella salina* and *Phaeodactylum tricornutum* cells grown in CTR, LL and PP conditions and analysed in the mid-exponential phase.

Table 7. Chlorophyll *a* and *b* content in *Tetraselmis suecica* and *Dunaliella salina*; and chlorophyll *a* and *c Phaeodactylum tricornutum* under different light regimes: CTR, LL and PP. Data are presented as mean ± standard deviations: n=10 for CTR and LL, n=8 for PP of *T. suecica*; n=6 for CTR and LL, n=8 for PP of *D. salina* and *P. tricornutum*. The statistical significance of the data was tested by a one-way ANOVA with Tukey-Kramer post-hoc test. Asterisks represent the

statistical significance of the chlorophyll content or ratio in LL and PP conditions with respect to that of CTR conditions (* = p < 0.05; ** = p < 0.01; *** = p < 0.001).

	Chl *a* (pg·cell^{-1})	**Chl *b* (*T. suecica, D. salina*) or Chl c_1+c_2 (*P. tricornutum*) (pg·cell^{-1})**	**Chl *a*:Chl *b* ratio (*T. suecica, D. salina*) or Chl *a*: Chl *c* ratio (*P. tricornutum*)**
***T. suecica* CTR**	1,57 (0,17)	0,88 (0,11)	1,80 (0,07)
***T. suecica* LL**	3,24 (0,34) ***	1,70 (0,18) ***	1,91 (0,02)
***T. suecica* PP**	1,29 (0,45)	0,65 (0,27)	2,07 (0,21) ***
***D. salina* CTR**	0,86 (0,15)	0,19 (0,03)	4,55 (0,17)
***D. salina* LL**	3,17 (0,42) ***	0,83 (0,11) ***	3,80 (0,04) ***
***D. salina* PP**	1,26 (0,23)	0,30 (0,05)	4,23 (0,11) ***
***P. tricornutum* CTR**	0,13 (0,01)	0,02 (0,001)	5,22 (0,31)
***P. tricornutum* LL**	0,35 (0,06) ***	0,06 (0,01) ***	5,77 (0,32)
***P. tricornutum* PP**	0,15 (0,03)	0,03 (0,02) ***	5,25 (1,21)

As shown in Table 7, the content of Chl *a* in *Tetraselmis suecica* CTR (1.6 pg·cell^{-1}) was almost halved in respect to LL (3.2 pg·cell^{-1}) , but slightly higher than in PP (1.3 pg·cell^{-1}). As for the Chl *b*, in CTR conditions was equal to 0.9 pg·cell^{-1}, in LL conditions was1.7 pg·cell^{-1}, and under PP, it was the half, showing the same trend as Chl *a*. The Chl *a* to Chl *b* ratio was similar in all light conditions ranging among about 1.8 in the CTR to about 2 in PP conditions.

In *Dunaliella salina*, results were in line with the ones of *T. suecica* above, with the LL sample characterized by the highest amount of both Chl *a* and Chl *b*. However, in *D. salina*, the Chl *a*:Chl *b* ratio showed higher variability among samples. It was the highest in CTR, being equal to 4.6, followed by PP and, the lowest in LL, with 3.8.

Phaeodactylum tricornutum had a very similar Chl *a* content in both CTR and PP (~0.15 pg·cell^{-1}). In LL, this content was approximately 2.5-fold higher. In parallel, the content of Chl c_1+c_2 was very low in CTR and PP, around 0.02 pg·cell^{-1}, whereas in LL, it was almost three times higher. The Chl *a*:Chl *c* ratio varied from about 5.2 in the CTR and about 5.8 in LL.

3.3. Cellular organic composition

The cellular organic composition was determined in *Tetraselmis suecica, Dunaliella salina* and *Phaeodactylum tricornutum* cells grown in CTR, LL and PP conditions and analysed from the mid-exponential growth.

3.3.1. Elemental composition

Elemental composition was investigated in *Tetraselmis suecica* and *Dunaliella salina* under CTR and LL conditions, focusing on C and N cell quota.

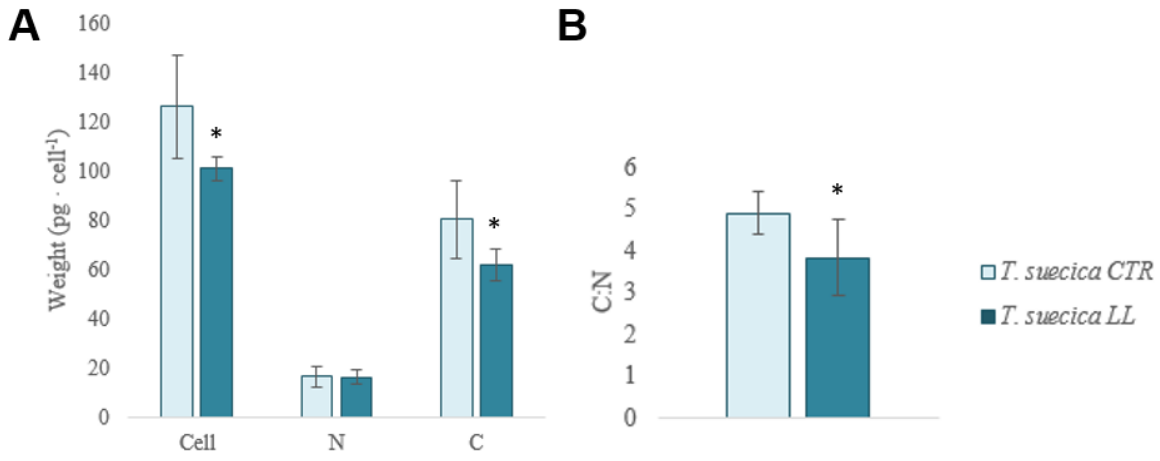

Figure 28. A) Cell dry weight, elemental nitrogen and carbon weight (pg·cell^{-1}) and B) carbon to nitrogen ratio of *Tetraselmis suecica* under CTR (light blue) and LL (dark blue). Data are presented as mean ± standard deviations (n=6 for CTR, n=5 for LL). The statistical significance of the data was tested by a one-way ANOVA. Asterisks represent the

statistical significance of the elemental composition and C/N ratio in LL conditions with respect to that of CTR conditions (* = p < 0.05; ** = p < 0.01; *** = p < 0.001).

Tetraselmis suecica CTR cells dry weight was 120 pg·cell^{-1}, 20 pg·cell^{-1} more than under LL conditions (Figure 28A). The same was observed in terms of carbon weight per cell, which was higher in CTR than in LL. The nitrogen content per cell, instead, stayed around 18 pg·cell^{-1} in both cases, and the C/N ratio was consistently different in the two conditions and equal to about 5 in CTR and 4 in LL (Figure 28B).

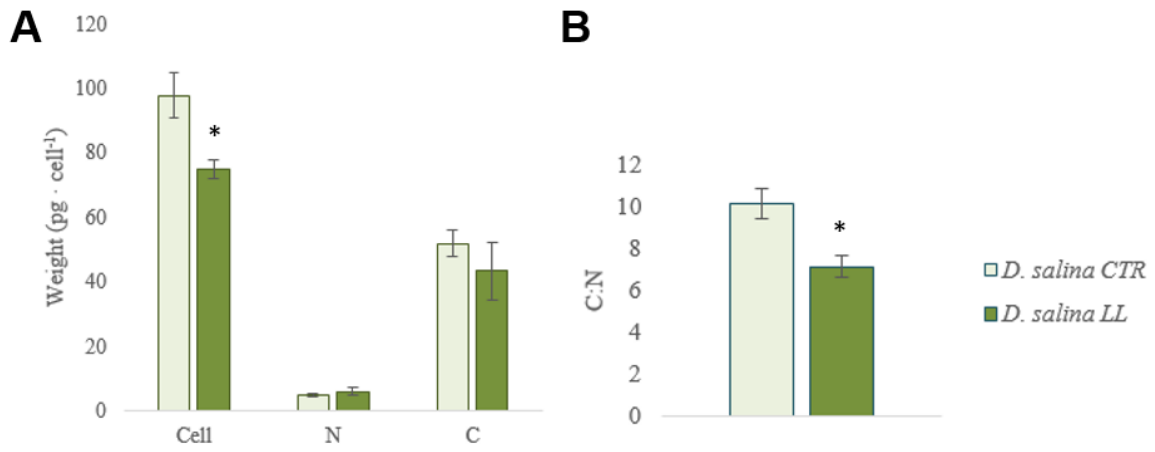

Figure 29. A) Cell dry weight, elemental nitrogen and carbon weight (pg·cell^{-1}) and B) carbon to nitrogen ratio of *Dunaliella salina* under CTR (light green) and LL (dark green). Data are presented as mean ± standard deviations (n=4 for CTR, n=6 for LL). The statistical significance of the data was tested by a one-way ANOVA. Asterisks represent the statistical significance of the elemental composition and C/N ratio in LL conditions with respect to that of CTR conditions (* = p < 0.05; ** = p < 0.01; *** = p < 0.001).

Similarly to what was observed in *T. suecica* above, the biomass and carbon content were higher in *D. salina* CTR. In Figure 29A, *Dunaliella salina* CTR cells weighted approximately 20% more than under LL. C cell quota showed a tendency to decrease as well in LL with respect to CTR, but the difference was not statistically significant. Cells acclimated to LL conditions had slightly more

nitrogen than CTR cells. The carbon to nitrogen ratio in *D. salina* CTR was 10, whereas in LL was one third lower (Figure 29B).

3.3.2. Quantification of proteins

Proteins were quantified in *Tetraselmis suecica, Dunaliella salina* and *Phaeodactylum tricornutum* acclimated to different light regimes.

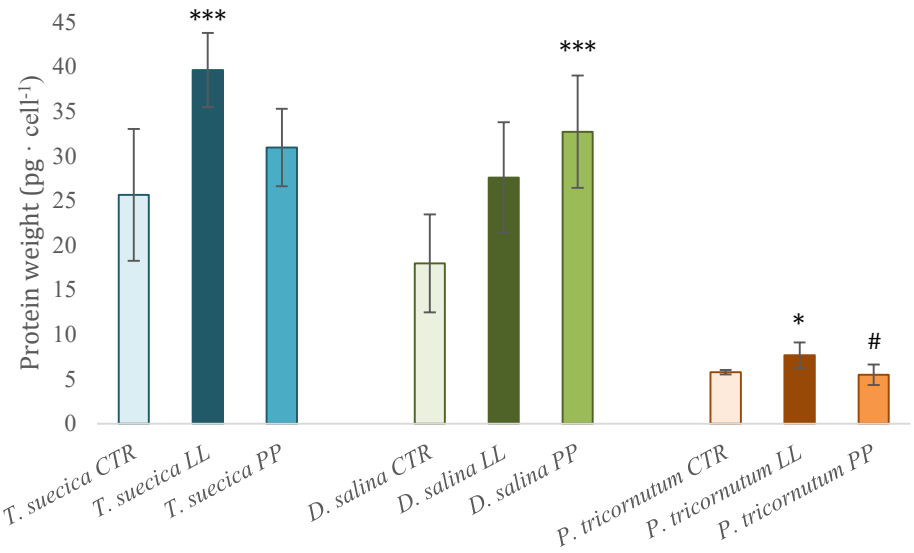

Figure 30. Quantification of proteins (pg·cell^{-1}) in *Tetraselmis suecica* (blue), *Dunaliella salina* (green) and *Phaeodactylum tricornutum* (orange) under CTR, LL and PP conditions. Data are presented as mean ± standard deviations: n=9 for CTR and LL, n=8 for LL in *T. suecica*; n=9 for CTR, n=6 for LL, n=8 for LL in *D. salina*; n=5 for CTR, n=4 for LL, n=6 for LL in *P. tricornutum*. The statistical significance of the data was tested by a one-way ANOVA with Tukey-Kramer post-hoc test. Asterisks represent the statistical significance of the amount of proteins in LL and PP conditions with respect to that of CTR conditions and the hashtags represent the the statistical significance in PP conditions with respect to that of LL conditions (* = $p < 0.05$; ** = $p < 0.01$; *** = $p < 0.001$).

The amount of proteins per cell in *Tetraselmis suecica* was similar in CTR (25 pg·cell^{-1}) and PP (30 pg·cell^{-1}) conditions. In LL instead, cells accumulated about 40 pg·cell^{-1} of proteins (Figure 30). Interestingly, the protein pool in *Dunaliella salina* varied differently among samples compared to

Tetraselmis suecica. The proteins amount was the lowest, less than 20 pg·cell^{-1}, in *D. salina* CTR cells and increased by 10 pg·cell^{-1} in LL, to become the highest under PP conditions, having almost 35 pg proteins per cell. The content of proteins in *Phaeodactylum tricornutum* was similar in CTR and PP conditions, being around 5 pg·cell^{-1}. Under LL, cells accumulated 3 pg·cell^{-1} of proteins more.

3.3.3. FTIR ratios, carbohydrates and lipid semiquantification

To gain also information on carbohydrates and lipid cell amount, macromolecular pools FTIR ratios were calculated in *Tetraselmis suecica, Dunaliella salina* and *Phaeodactylum tricornutum* acclimated to different light regimes and used to semiquantitatively evaluate the relative amount of carbohydrates and lipids in each species with respect to their control samples. Also, the values obtained reported in the following figures were normalized to the CTR, set to one.

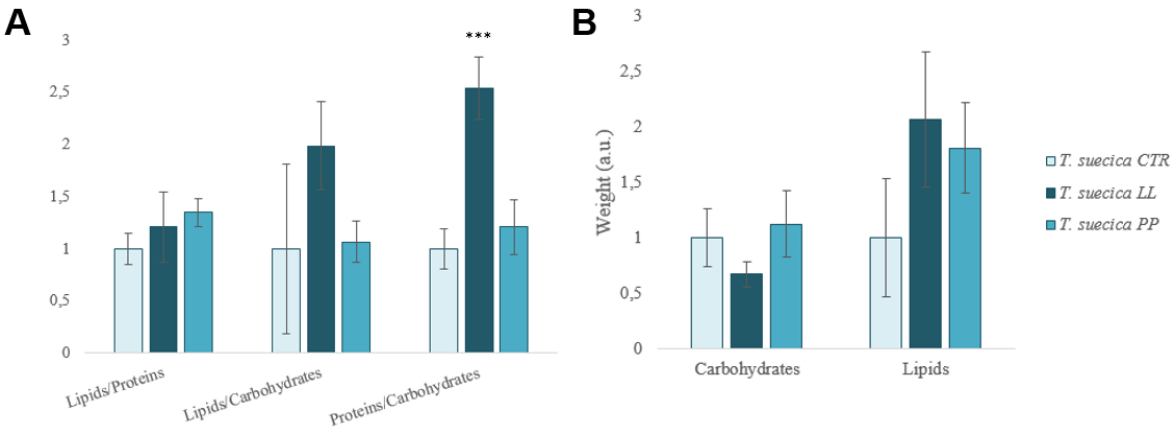

Figure 31. A) Macromolecular FTIR ratios and B) semiquantification of carbohydrates and lipids (expressed as arbitrary units (a.u.)) of *Tetraselmis suecica* under CTR, LL and PP conditions. The values norm is 1 in CTR. Data are presented as mean ± standard deviations: n=14 for CTR, n=12 for LL, n=8 for LL for macromolecular FTIR ratios; n=9 for CTR and LL, n=8 for LL for semiquantification of pools. The statistical significance of the data was tested by a one-way ANOVA with Tukey-Kramer post-hoc test. Asterisks represent the statistical significance of the macromolecular FTIR ratios and

semiquantifications of carbohydrates and lipids in LL and PP conditions with respect to that of control conditions (* = $p < 0.05$; ** = $p < 0.01$; *** = $p < 0.001$).

In Figure 31A and B, results for *Tetraselmis suecica* cells are shown. Lipids/proteins ratio was similar in all light conditions tested, while lipids/carbohydrates and proteins/carbohydrates showed a similar trend, with CTR and PP ratio roughly equal and LL samples showing a 2-fold increase. However, only the protein/carbohydrate ratio was statistically different in LL compared to CTR.

Based on these ratios and the absolute amount of proteins quantification, also the amount of carbohydrates and lipid pools can be estimated, relative to the CTR. Carbohydrates pool was slightly diminished in the LL compared to both CTR and PP, which, conversely, was the condition accumulating the highest amount of lipids. Despite some trend in favouring lipid accumulation over carbohydrates in LL can be seen, neither carbohydrates or lipid cell quotas showed statistically significant differences among the samples analysed and more experimental replicas should be analysed in order to understand whether the content of lipids is significantly lower in CTR than the other two conditions.

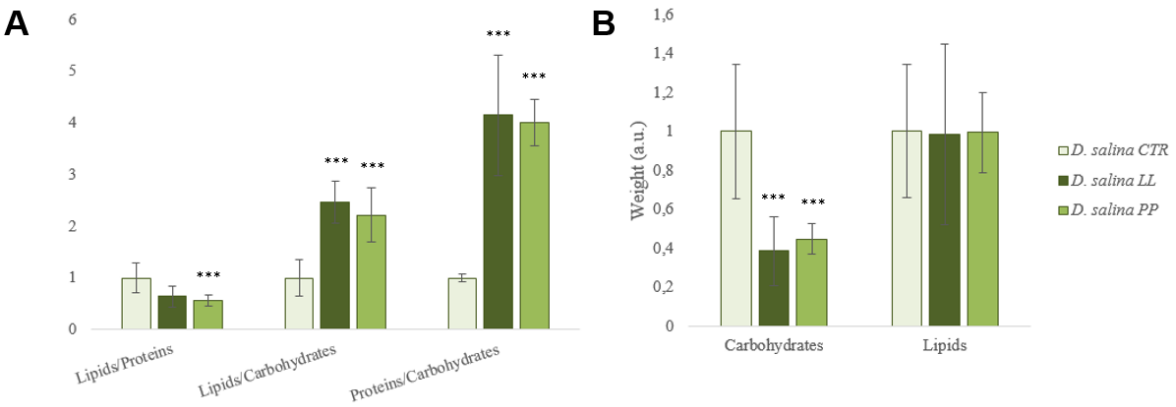

Figure 32. A) Macromolecular FTIR ratios and B) semiquantification of carbohydrates and lipids (expressed as arbitrary units (a.u.)) of *Dunaliella salina* under CTR, LL and PP conditions. The values norm is 1 in CTR. Data are presented as mean ± standard deviations: n=18 for CTR, n=16 for LL, n=8 for LL for macromolecular FTIR ratios; n=9 for CTR, n=6 for LL, n=8 for LL for semiquantification of pools. The statistical significance of the data was tested by a one-way ANOVA with Tukey-Kramer post-hoc test. Asterisks represent the statistical significance of the macromolecular FTIR ratios and

semiquantifications of carbohydrates and lipids in LL and PP conditions with respect to that of control conditions (* = $p < 0.05$; ** = $p < 0.01$; *** = $p < 0.001$).

In *Dunaliella salina* CTR, the lipids/proteins ratio was the highest among the conditions (Figure 32A), whereas a small change was observed between LL and PP, both were almost the half of that in CTR. LL and PP samples showed similar values as compared to CTR also for lipids/carbohydrates and proteins/carbohydrates, but in these cases the ratio values of both LL and PP were 2.5-fold higher in lipids/carbohydrates and 4-fold higher in proteins/carbohydrates, respectively, with respect to the CTR. As seen in Figure 32B, the carbohydrate pool more than doubled in CTR compared to LL and PP conditions. The content of lipids was instead roughly the same in all three regimes.

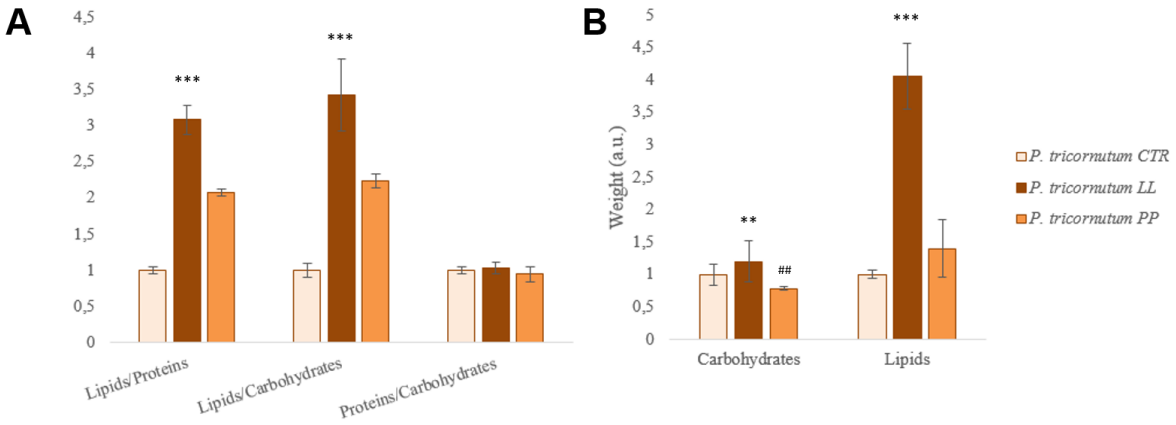

Figure 33. A) Macromolecular FTIR ratios and B) semiquantification of carbohydrates and lipids (expressed as arbitrary units (a.u.)) of *Phaeodactylum tricornutum* under CTR, LL and PP conditions. The values norm is 1 in CTR. Data are presented as mean ± standard deviations: n=5 for CTR, n=4 for LL, n=6 for LL for macromolecular FTIR ratios; n=5 for CTR, n=4 for LL, n=6 for LL for semiquantification of pools. The statistical significance of the data was tested by a one-way ANOVA with Tukey-Kramer post-hoc test. Asterisks represent the statistical significance of the macromolecular FTIR ratios and semiquantifications of carbohydrates and lipids in LL and PP conditions with respect to that of control conditions

and the hashtags represent the the statistical significance in PP conditions with respect to that of LL conditions (* = $p < 0.05$; ** = $p < 0.01$; *** = $p < 0.001$).

As Figure 33 shows, the lipids/proteins and lipids/carbohydrates ratios varied among the three conditions of *Phaeodactylum tricornutum*. In the first case, under CTR, lipids to proteins were three times lower than in LL, and under PP, the values were the double compared to the CTR. In the second case, lipids to carbohydrates was almost 3.5 times more elevated in LL than in CTR, whereas in PP the ratio had a similar value than in the lipids/proteins ratio. As for the proteins/carbohydrates ratio, the values were similar among all conditions. The quantity of carbohydrates per cell did not vary much among the three conditions of light. *Phaeodactylum tricornutum* accumulated the least lipids in CTR conditions. Under LL, cells managed to store 4-fold more lipids than in CTR, and a 40% increase compared to CTR occurred in PP.

DISCUSSION AND CONSCLUSIONS

Photosynthesis is diversified in the three species investigated

Although PS reaction centers are widely conserved among oxygenic photosynthetic organisms, the light harvesting apparatus, the specific pigments bound (in addition to Chl *a*), and the regulation of light harvesting and photosynthetic electron transport adapted during evolution of photosynthetic organisms (Peltier et al., 2010; Allen et al., 2011; Niyogi & Truong, 2013; Allahverdiyeva et al., 2015).

We here analyzed the acclimation of three marine microalgae species, two chlorophytes (*Tetraselmis suecica* and *Dunaliella salina*, harboring Chl *a* and *b*) and the model diatom *Phaeodactylum tricornutum* (with Chl *a* and *c*). In addition to the obvious above mentioned differences in photosynthetic pigments due to their different phylogeny (LEWIN, 1958; Leliaert et al., 2012; Borowitzka & Siva, 2007; Howe et al., 2008), the *in vivo* characterization of photosynthesis by means of light curves protocols and presented in Figure 16-Figure 27 allowed to gain insights on the dynamic responses of photosynthesis to light changes in the three species under investigation. Figure 34 compares the NPQ parameter from CTR sample of the 3 species (see also Figure 22-Figure 24). In all species, it increased in response to increasing light used in the analyses (Figure 22-Figure 24). Yet, the specific light intensity required for activation, amplitude and kinetic of the NPQ parameter was diversified among the samples. This is not unique to our work, variability of microalgal NPQ amplitude and kinetic has already been recognized (Gerotto & Morosinotto, 2013). Non-photochemical quenching (NPQ) is, from the physiological processes' point of view, a very complex parameter which includes multiple molecular mechanisms which results in a "non-photochemical" (i.e. not driving charge separation and electron transport) quenching of chlorophyll fluorescence. Frequently, the main components of NPQ are the pH-dependent processes involved in the dissipation as heat of exceeding energy absorbed. They are fastly activated (seconds or minutes timescale) in the

light and quickly relaxed in the dark, and depend on specific LHC-like proteins (LHCSR in green algae and LHCX in diatoms; Peers et al., 2009; Bailleul et al., 2010) and on the reversible accumulation of specific carotenoids, like zeaxanthin and diatoxanthin in diatoms (Lacour et al., 2020). Despite both processes have been shown to contribute in different species, substantial species-specific differences also emerged (Hosseini Tafreshi & Shariati, 2009; Peers et al., 2009; Bailleul et al., 2010; Lavaud & Goss, 2014; Abu-Ghosh et al., 2015; Berne et al., 2018; Lacour et al., 2020). In *P. tricornutum*, the contribution of LHCX proteins and DD/DDT xanthophyll cycle is well known (Buck et al., 2019; Goss et al., 2006), and NPQ activation in our *P. tricornutum* CTR samples consistently shows a fast induction starting from 300 $\mu mol \cdot m^2 \cdot s^{-1}$, reaching a saturation at 1031 $\mu mol \cdot m^2 \cdot s^{-1}$. *T. suecica* photosynthetic apparatus, conversely, is still poorly characterized. In *T. suecica*, the NPQ increased almost linearly till 342 $\mu mol \cdot m^2 \cdot s^{-1}$ to then reach saturation, and was characterized by a minor amplitude compared to *P. tricortnutum*. Yet, the NPQ relaxed in less than 1 minute upon a shift from light to dark, as demonstrated in Figure 35, where *T. suecica* cells were exposed to 5 minutes of light which was then switched off. This suggests that the pH-dependent components described above are the main molecular mechanisms activated to regulate photosynthesis in our *T. suecica* cells. As opposite, in *D. salina*, NPQ showed a first peak of induction soon after light was switched on, then relaxed to increase again (Figure 34). The light-dark cycle in Figure 35 further infers the NPQ contributions in *D. salina* to be more complex than in the other two species with more, or different, physiological processes which come into play. The NPQ parameter, consistently, also includes lasting quenching mechanisms, and any processes which result in a decreased Chl fluorescence yield in PSII, like the induction of state transition, or processes which temporarily modify luminal pH due to altered electron transport and induce the pH-dependent energy quenching explained above (Müller et al., 2001; Murchie & Lawson, 2013). The amplitude of such mechanisms varies substantially among species, but in the case of *D. salina*, Thaipratum and co-workers (in 2009) consistently showed that, when light is too low to induce pH-dependent mechanisms, state transition is induced in *D. salina*.

The differences in NPQ are reflected by time-course changes in the other parameters analyzed, like Y(II), which showed a temporary increase in *D. salina* concomitantly with the relaxation of NPQ (70 $\mu mol \cdot m^2 \cdot s^{-1}$).

The observed differences in NPQ kinetics among the microalgae studied, thus, are likely to be related to differences in their photosynthetic apparatus and its regulation/photoprotection mechanisms, which themselves might be related to species-specific ecological niches. *T. suecica* photosynthetic apparatus characterization is still lacunous, while more studies focused on *D. salina* and *P. tricornutum*. For example, the latter two species are known to harbor differences in the PSI structure (Depauw et al., 2012; Perez-Boerema et al., 2020). Yet, uncovering the physiological reason of the low F_v/F_m in CTR in all species, and a more accurate identification of the contributions of photoprotection/regulatory mechanisms leading to the diversified kinetics obtained, require more in-depth analyses of photosynthesis in the analyzed microalgae in our growth conditions.

In addition to specific dynamics of photosynthetic electron transport upon fast light changes, also acclimation of the cultures to different light regimes showed some differences. Although all the species grown in LL increased their chlorophylls accumulation per cell (i.e., accumulating more LHC and PS), a common strategy for photosynthetic cells to enlarge their capacity to harvest photons, the Chl *a*/*b* (in *T. suecica* and *D. salina*) and Chl *a*/*c* (*P. tricornutum*) ratio varied differently. In *T suecica* and *P. tricornutum*, Chl *a*/accessory Chl ratio was similar to that of CTR, while in *D. salina* it decreased significantly. This suggests that in *D. salina,* the photosynthetic apparatus in LL also changed qualitatively as compared to CTR, by changing the LHC/PS ratio (as suggested by a decrease Chl *a*/*b* ratio, being Chl *b* bound to LHC) and /or the PSII/PSI ratio. Biochemical characterization of the photosynthetic apparatus will allow to confirm the specific changes in the species.

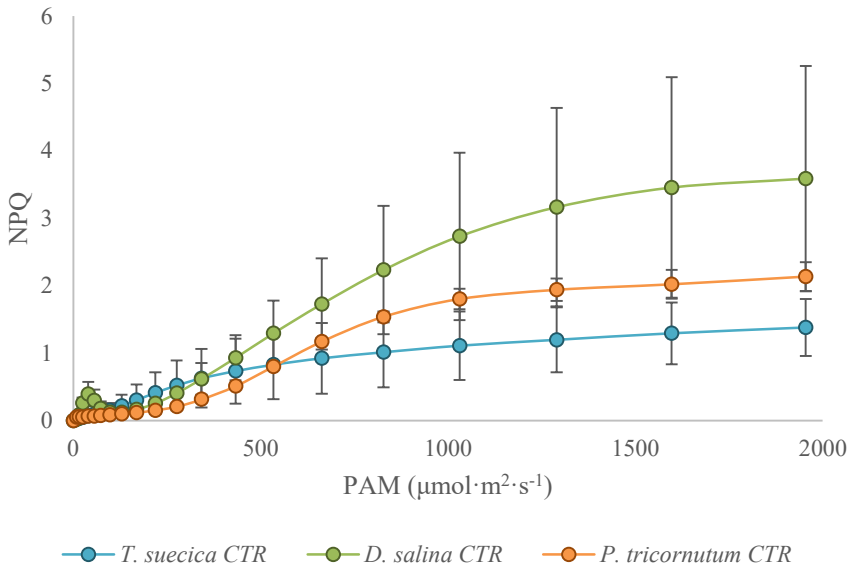

Figure 34. Non-photochemical quenching (NPQ) of *Tetraselmis suecica*, *Dunaliella salina* and *Phaeodactylum tricornutum* under control conditions from Figure 22-Figure 24. Data are presented as mean ± standard deviations (n=4 for *T. suecica*, n=6 for *D. salina* and *P. tricornutum*).

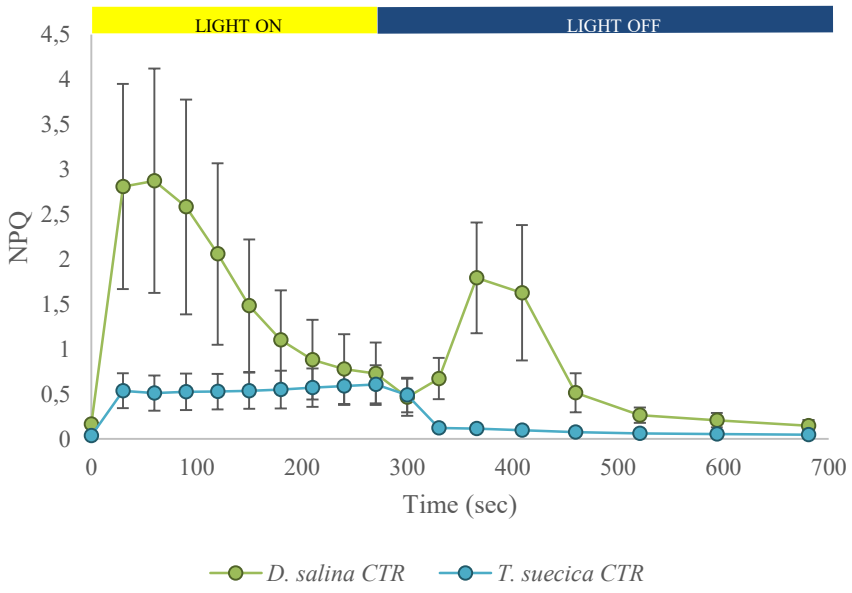

Figure 35. Non-photochemical quenching (NPQ) of induction kinetics of *Tetraselmis suecica and Dunaliella salina* under control conditions. In the first 270 seconds, the light was swithched on and was switched off after. Data are presented as mean ± standard deviations (n=3 for *T. suecica;* n=5 for *D. salina*).

Microalgal species analysed acclimated their photosynthesis to low light but were characterized by a different C and energy allocation

A significantly higher chlorophyll content in *T. suecica*, D. *salina* and *P. tricornutum* under LL conditions than in control conditions was found together with a higher amount of proteins. The decrease of the C/N ratio (Figure 28, Figure 29) confirmed the allocation of a larger proportion of C into the N containing molecular pool, proteins. It is likely that more protein complexes of the photosynthetic apparatur were required to improve photon capture and photosynthetic efficiency, as suggested in the paragraph above (Figure 15; Borghini et al., 2009; Li et al., 2019; Nagao et al., 2019). Yet, protein synthesis is more energy-demanding than other macromolecular pools, as it requires the assimilation of N and S, in addition to C fixation. Nevertheless, LL cells invested their energy for the synthesis of this pool. The lower growth rate observed (Figure 14) both in *D. salina* and *P. tricornutum*, and also in *T. suecica* (even if not statistically different from CTR) under LL regime, together with the lower cell dry weight (Figure 28,Figure 29), may be explained as the cost to redirect resources into the protein pool at the expences of biomass accumulation and other macromolecules, i.e. carbohydrates, during acclamatory response to LL regime (Giordano, 2013). In particular, *D. salina* showed half the content of carbohydrates in LL with respect to CTR cells (Figure 31-Figure 33).

Further, since the protein complexes are held in thylakoidal membranes, that are constituted by polar lipids, like glycolipids and phospholipids, the higher lipid pool observed in *T. suecica* and *P. tricornutum* could be at least in part due to carbon reallocation into the production of these lipids as already proposed (Kumari et al., 2013; Fernandes et al., 2016). In addition, both the species are known to be oleaginous algae: they allocate fixed carbon preferentially into lipids rather than into carbohydrates as carbon storage (Carballo-Cárdenas et al., 2003; Griffiths & Harrison, 2009; Go et al., 2012).

Macromolecular composition varies according to phylogenetic groups (Finkel et al., 2016) and environmental or energy availability. In fact, the allocation of C to either carbohydrates or lipids, however, is not energetically equivalent (Montechiaro et al., 2006; Raven, 2005) : while the incorporation of 1 mole of C into starch requires 3.17 mol of ATP and 2 mol of NADPH, the fixation of an equal amount of C into tripalmityl glycerol requires 3.88 mol of ATP and 2.84 mof of NADPH. When energy is available, the allocation of carbon into lipids rather than into carbohydrates gives the advantage of a higher energy pool per unit of volume, C, and mass (Raven, 2005; Schmidt Nielsen et al., 1983). Especially *P. tricornutum*, having a smaller volume than the other experimental species, as well as showing a further volume reduction under LL conditions as compared to the one in CTR (data not shown), may have benefits from storage lipids. It is still surprising that lipids accumulated at the LL condition in the diatom; further work is needed to investigate such response.

Finally, we started the characterization of cells under photoperiod growth conditions. The decrease in growth rate as compared to CTR cells can be explained with the total amount of photons received by the cells: despite the light intensity applied was the same in CTR and PP, the 12h:12h photoperiod resulted in half as much photons available for the PP cultures during the 24 hours. As for the cell quota of proteins and carbohydrates in *D. salina*, despite the trend is the same of LL, the underlying physiological reasons might be different. PP condition did not result in a strong increase in the chlorophyll amount per cell as in LL, implying no need for a more efficient photosynthetic apparatus in terms of photon capture. However, in PP conditions, the increased protein pool may serve in metabolic pathways, different than photosynthesis, activated by cells during the 12 hours of dark (Mackinder et al., 2014; Sui et al., 2019). However, to verify this hypothesis, proteomic studies should be performed in the future. A change in metabolism from light to dark can also explain the lower carbohydrate content under photoperiod regime. Part of the carbohydrates produced over the 12 hours of light is most likely consumed during the 12 hours of darkness, when photosynthesis is inactive and only respiration occurs (Edmundson & Huesemann, 2015). A time course of carbohydrates quantification during the 24 hours might help in verifying this hypothesis.

Overall, the experiment presented here showed that different microalgae display a diversified acclimation response to different light regimes. Even the two green algae belonging to the same phylogenetic groups has a species-specific response. *T. suecica* showed a more homeostatic behaviour, keeping the different macromolecular pools relatively stable under the different growth regimes. Indeed, even when increasing the chlorophyll (and thus proteins) content per cell, the Chl *a*/*b* ratio was kept rather constant, suggesting that, although the amount of photosynthetic apparatus subunits was higher, their relative ratio was kept the same irrespective of the growth conditions. Conversely, *D. salina* showed an acclamatory response to the external challenges. This was seen in light curve experiment, showing a very dynamic response of electron transport upon short tern changes in light, up to the changes in energy and C allocation, as revealed by the changes in macromolecular pools.

ACKNOWLEDGEMENTS

I thank all my family and friends who have supported me on every step of the way while studying abroad. I especially thank my mother; to whom I will be forever grateful for the incredible support in following my dreams.

I thank my co-relator, dott. Caterina Gerotto, who has helped me to better understand what research is all about and who has kept me motivated throughout the completion of the thesis. I also thank my former relator, prof. Mario Giordano, who accepted me as his graduate student, but, unfortunately, passed away during the on-going of the thesis. And I thank my latter relator, prof. Alessandra Norici, for great advice and management of the laboratory, even after what happened.

I thank my dear friend and laboratory mate, Maria Bruno, for being there for me in the best and the worst moments of the time I had spent in Ancona. The many thanks also go to all my laboratory colleagues: Daniel Kurpan and Alessandra Petrucciani, who taught me how to use most of the laboratory equipment and were giving me good advices, as well as Lorenzo Mollo and Stefano Maso.

REFERENCES

Abu-Ghosh, S., Fixler, D., Dubinsky, Z., Solovchenko, A., Zigman, M., Yehoshua, Y., & Iluz, D. (2015). Flashing light enhancement of photosynthesis and growth occurs when photochemistry and photoprotection are balanced in Dunaliella salina. *European Journal of Phycology*, *50*(4), 469–480. https://doi.org/10.1080/09670262.2015.1069404

Allahverdiyeva, Y., Suorsa, M., Tikkanen, M., & Aro, E. M. (2015). Photoprotection of photosystems in fluctuating light intensities. *Journal of Experimental Botany*, *66*(9), 2427–2436. https://doi.org/10.1093/jxb/eru463

Allen, J. F., de Paula, W. B. M., Puthiyaveetil, S., & Nield, J. (2011). A structural phylogenetic map for chloroplast photosynthesis. *Trends in Plant Science*, *16*(12), 645–655. https://doi.org/10.1016/j.tplants.2011.10.004

Álvarez, E., Thoms, S., Bracher, A., Liu, Y., & Völker, C. (2019). Modeling Photoprotection at Global Scale: The Relative Role of Nonphotosynthetic Pigments, Physiological State, and Species Composition. *Global Biogeochemical Cycles*, *33*(7), 904–926. https://doi.org/10.1029/2018GB006101

Armbrust, E. V. (2009). The life of diatoms in the world's oceans. *Nature*, *459*(7244), 185–192. https://doi.org/10.1038/nature08057

Bailleul, B., Rogato, A., De Martino, A., Coesel, S., Cardol, P., Bowler, C., Falciatore, A., & Finazzi, G. (2010). An atypical member of the light-harvesting complex stress-related protein family modulates diatom responses to light. *Proceedings of the National Academy of Sciences of the United States of America*, *107*(42), 18214–18219. https://doi.org/10.1073/pnas.1007703107

Baker, N. R. (1989). electron transport and quenching of chlorophyll fluorescence. *BBA - General Subjects*, *990*(1), 87–92. https://doi.org/10.1016/S0304-4165(89)80016-9

Baker, N. R. (2008). Chlorophyll fluorescence: A probe of photosynthesis in vivo. *Annual Review of Plant Biology*, *59*, 89–113. https://doi.org/10.1146/annurev.arplant.59.032607.092759

Barber, J., & Archer, M. D. (2001). P680, the primary electron donor of photosystem II. *Journal of Photochemistry and Photobiology A: Chemistry*, *142*(2–3), 97–106. https://doi.org/10.1016/S1010-6030(01)00503-2

Berne, N., Fabryova, T., Istaz, B., Cardol, P., & Bailleul, B. (2018). The peculiar NPQ regulation in the stramenopile Phaeomonas sp. challenges the xanthophyll cycle dogma. *Biochimica et Biophysica Acta - Bioenergetics*, *1859*(7), 491–500. https://doi.org/10.1016/j.bbabio.2018.03.013

Björn, L. O., Papageorgiou, G. C., Blankenship, R. E., & Govindjee. (2009). A viewpoint: Why

chlorophyll a? *Photosynthesis Research*, *99*(2), 85–98. https://doi.org/10.1007/s11120-008-9395-x

Bo, U., Lillehaug, D., & Martens, H. (2010). *A high-throughput microcultivation protocol for FTIR spectroscopic characterization*. *521*(8), 512–521. https://doi.org/10.1002/jbio.201000014

Bohlin, K. (1898 '1897'). Zur Morphologie und Biologie einzelliger Algen. Öfversigt af Kongliga [Svenska] Vetenskadademiens Förhanligar, Stockholm 54: 507-529.

Bolhàr-Nordenkampf, H. R., & Öquist, G. (1993). Chlorophyll fluorescence as a tool in photosynthesis research BT - Photosynthesis and Production in a Changing Environment: A field and laboratory manual. *Photosynthesis and Production in a Changing Environment*, 193–206. https://doi.org/10.1007/978-94-011-1566-7_12

Borghini, F., Colacevich, A., Bergamino, N., Micarelli, P., Dattilo, A. M., Focardi, S., Focardi, S., & Loiselle, S. A. (2009). The microalgae Tetraselmis suecica in mesocosms under different light regimes. *Chemistry and Ecology*, *25*(5), 345–357. https://doi.org/10.1080/02757540903193148

Borowitzka, M. A., & Siva, C. J. (2007). The taxonomy of the genus Dunaliella (Chlorophyta, Dunaliellales) with emphasis on the marine and halophilic species. *Journal of Applied Phycology*, *19*(5), 567–590. https://doi.org/10.1007/s10811-007-9171-x

Bowler, C., & Falciatore, A. (2019). Phaeodactylum tricornutum. *Trends in Genetics*, *35*(9), 706–707. https://doi.org/10.1016/j.tig.2019.05.007

Buchanan, B. B. (2016). The carbon (formerly dark) reactions of photosynthesis. *Photosynthesis Research*, *128*(2), 215–217. https://doi.org/10.1007/s11120-015-0212-z

Buck, J. M., Sherman, J., Bártulos, C. R., Serif, M., Halder, M., Henkel, J., Falciatore, A., Lavaud, J., Gorbunov, M. Y., Kroth, P. G., Falkowski, P. G., & Lepetit, B. (n.d.). dissipation of absorbed light in the diatom. *Nature Communications*, *2019*. https://doi.org/10.1038/s41467-019-12043-6

Buick, R. (2008). *When did oxygenic photosynthesis evolve ? May*, 2731–2743. https://doi.org/10.1098/rstb.2008.0041

Carballo-Cárdenas, E. C., Tuan, P. M., Janssen, M., & Wijffels, R. H. (2003). Vitamin E (α-tocopherol) production by the marine microalgae Dunaliella tertiolecta and Tetraselmis suecica in batch cultivation. *Biomolecular Engineering*, *20*(4–6), 139–147. https://doi.org/10.1016/S1389-0344(03)00040-6

Cardona, T., Shao, S., & Nixon, P. J. (2018). Enhancing photosynthesis in plants: the light reactions. *Essays in Biochemistry*, *62*(1), 85–94. https://doi.org/10.1042/EBC20170015

Chen, M., & Blankenship, R. E. (2011). Expanding the solar spectrum used by photosynthesis.

Trends in Plant Science, *16*(8), 427–431. https://doi.org/10.1016/j.tplants.2011.03.011

Cowan, A. K., Rose, P. D., & Horne, L. G. (1992). Dunaliella salina: A model system for studying the response of plant cells to stress. *Journal of Experimental Botany*, *43*(12), 1535–1547. https://doi.org/10.1093/jxb/43.12.1535

Croce, R., Müller, M. G., Bassi, R., & Holzwarth, A. R. (2001). Carotenoid-to-chlorophyll energy transfer in recombinant major light-harvesting complex (LHCII) of higher plants. I. Femtosecond transient absorption measurements. *Biophysical Journal*, *80*(2), 901–915. https://doi.org/10.1016/S0006-3495(01)76069-9

Depauw, F. A., Rogato, A., D'Alcalá, M. R., & Falciatore, A. (2012). Exploring the molecular basis of responses to light in marine diatoms. *Journal of Experimental Botany*, *63*(4), 1575–1591. https://doi.org/10.1093/jxb/ers005

Dilek (Yalcin) Duygu,. (2012). Fourier transform infrared (FTIR) spectroscopy for identification of Chlorella vulgaris Beijerinck 1890 and Scenedesmus obliquus (Turpin) Kützing 1833. *African Journal of Biotechnology*, *11*(16), 3817–3824. https://doi.org/10.5897/ajb11.1863

Domenighini, A., & Giordano, M. (2009). Fourier transform infrared spectroscopy of microalgae as a novel tool for biodiversity studies, species identification, and the assessment of water quality. *Journal of Phycology*, *45*(2), 522–531. https://doi.org/10.1111/j.1529-8817.2009.00662.x

Domozych, D. S., Stewart, K. D., & Mattox, K. R. (1981). Development of the cell wall in tetraselmis: role of the Golgi apparatus and extracellular wall assembly. *Journal of Cell Science*, *Vol. 52*, 351–371.

Dougherty, R. C., Strain, H., Svec, W. A., Uphaus, R. A., & Katz, J. J. (1970). *The Structure , Properties , and Distribution of Chlorophyll c*. *271*(8), 2826–2833. https://doi.org/10.1021/ja00712a037

Dubinsky, Z., & Stambler, N. (2009). *Photoacclimation processes in phytoplankton : mechanisms , consequences , and applications*. *56*(September), 163–176. https://doi.org/10.3354/ame01345

Ecology, P. P. (2008). *Photosynthesis, Respiration, and Long-Distance Transport*. https://doi.org/10.1007/978-0-387-78341-3

Edmundson, S. J., & Huesemann, M. H. (2015). The dark side of algae cultivation: Characterizing night biomass loss in three photosynthetic algae, Chlorella sorokiniana, Nannochloropsis salina and Picochlorum sp. *Algal Research*, *12*, 470–476. https://doi.org/10.1016/j.algal.2015.10.012

Einspahr, K. J., Maeda, M., & Thompson, G. A. (1988). *Concurrent Changes in*. *107*(August), 529–538.

Fabregas, J., Abalde, J., Herrero, C., Cabezas, B., & Veiga, M. (1984). Growth of the marine microalga Tetraselmis suecica in batch cultures with different salinities and nutrient

concentrations. *Aquaculture*, *42*(3–4), 207–215. https://doi.org/10.1016/0044-8486(84)90101-7

Fernandes, T., Fernandes, I., Andrade, C. A. P., & Cordeiro, N. (2016). Marine microalgae growth and carbon partitioning as a function of nutrient availability. *Bioresource Technology*, *214*, 541–547. https://doi.org/10.1016/j.biortech.2016.05.001

Ficek, D., Majchrowski, R., Ostrowska, M., & Woźniak, B. (2000). Influence of non-photosynthetic pigments on the measured quantum yield of photosynthesis. *Oceanologia*, *42*(2), 231–242.

Finkel, Z. V., Follows, M. J., Liefer, J. D., Brown, C. M., Benner, I., & Irwin, A. J. (2016). Phylogenetic diversity in the macromolecular composition of microalgae. *PLoS ONE*, *11*(5), 1–16. https://doi.org/10.1371/journal.pone.0155977

Geider, R. J., Delucia, E. H., Falkowski, P. G., Finzi, A. C., Philip Grime, J., Grace, J., Kana, T. M., La Roche, J., Long, S. P., Osborne, B. A., Platt, T., Colin Prentice, I., Raven, J. A., Schlesinger, W. H., Smetacek, V., Stuart, V., Sathyendranath, S., Thomas, R. B., Vogelmann, T. C., … Ian Woodward, F. (2001). Primary productivity of planet earth: Biological determinants and physical constraints in terrestrial and aquatic habitats. *Global Change Biology*, *7*(8), 849–882. https://doi.org/10.1046/j.1365-2486.2001.00448.x

Gerotto, C., & Morosinotto, T. (2013). Evolution of photoprotection mechanisms upon land colonization: Evidence of PSBS-dependent NPQ in late Streptophyte algae. *Physiologia Plantarum*, *149*(4), 583–598. https://doi.org/10.1111/ppl.12070

Giordano, M. (2013). Homeostasis: An underestimated focal point of ecology and evolution. *Plant Science*, *211*, 92–101. https://doi.org/10.1016/j.plantsci.2013.07.008

Giordano, M., Heraud, P., Beardall, J., Giordano, M., & Al, E. T. (2001). *FOURIER TRANSFORM INFRARED SPECTROSCOPY AS A NOVEL TOOL TO INVESTIGATE CHANGES IN INTRACELLULAR MACROMOLECULAR POOLS IN THE MARINE MICROALGA CHAETOCEROS MUELLERII (BACILLARIOPHYCEAE) 1 Fourier Transform Infrared (FT-IR) spectroscopy was used to study* . *279*, 271–279.

Giordano, M., Ratti, S., Domenighini, A., & Vogt, F. (2009). Spectroscopic classification of 14 different microalga species: First steps towards spectroscopic measurement of phytoplankton biodiversity. *Plant Ecology and Diversity*, *2*(2), 155–164. https://doi.org/10.1080/17550870903353088

Gnaiger, E., Bitterlich, G., & Composition, P. B. (2012). Original papers Proximate biochemical composition and caloric content calculated from elemental CHN analysis : a stoichiometric concept. *International Association for Ecology*, *62*(3), 289–298.

Go, S., Lee, S. J., Jeong, G. T., & Kim, S. K. (2012). Factors affecting the growth and the oil

accumulation of marine microalgae, Tetraselmis suecica. *Bioprocess and Biosystems Engineering*, *35*(1–2), 145–150. https://doi.org/10.1007/s00449-011-0635-7

Goss, R., Ann, E., Wilhelm, C., & Richter, M. (2006). *The importance of a highly active and D pH-regulated diatoxanthin epoxidase for the regulation of the PS II antenna function in diadinoxanthin cycle containing algae*. *163*, 1008–1021. https://doi.org/10.1016/j.jplph.2005.09.008

Granick, S. (n.d.). Evolution of Heme and Chlorophyll. In *EVOLVING GENES AND PROTEINS: A SYMPOSIUM Held at the Institute of Microbiology of Rutgers · The State University with support from the NATIONAL SCIENCE FOUNDATION*. ACADEMIC PRESS INC. https://doi.org/10.1016/B978-1-4832-2734-4.50014-0

Green, B. R., Anderson, J. M., & Parson, W. W. (2003). *Chapter 1 Photosynthetic Membranes and Their Light-Harvesting Antennas*. 1–28.

Griffiths, M. J., & Harrison, S. T. L. (2009). Lipid productivity as a key characteristic for choosing algal species for biodiesel production. *Journal of Applied Phycology*, *21*(5), 493–507. https://doi.org/10.1007/s10811-008-9392-7

Hamilton, T. L. (2019). Free Radical Biology and Medicine The trouble with oxygen : The ecophysiology of extant phototrophs and implications for the evolution of oxygenic photosynthesis. *Free Radical Biology and Medicine*, *140*(April), 233–249. https://doi.org/10.1016/j.freeradbiomed.2019.05.003

Hartmann, P., Nikolaou, A., & Bernard, O. (2013). *A Dynamic Model coupling Photoacclimation and Photoinhibition in Microalgae*. 4178–4183.

Heinz Walz, & Walz, H. (2006). Dual-PAM-100 Measuring System for Simultaneous Assessment of P700 and Chlorophyll Fluorescence. *System*, *1e*.

Hirschmugl, C. J., Bayarri, Z. El, Bunta, M., Holt, J. B., & Giordano, M. (2006). Analysis of the nutritional status of algae by Fourier transform infrared chemical imaging. *Infrared Physics and Technology*, *49*(1–2), 57–63. https://doi.org/10.1016/j.infrared.2006.01.032

Hosseini Tafreshi, A., & Shariati, M. (2009). Dunaliella biotechnology: Methods and applications. *Journal of Applied Microbiology*, *107*(1), 14–35. https://doi.org/10.1111/j.1365-2672.2009.04153.x

Howe, C. J., Barbrook, A. C., Nisbet, R. E. R., Lockhart, P. J., & Larkum, A. W. D. (2008). The origin of plastids. *Philosophical Transactions of the Royal Society B: Biological Sciences*, *363*(1504), 2675–2685. https://doi.org/10.1098/rstb.2008.0050

Iii, W. W. A. (1973). *The xanthophyll cycle*. *1959*.

Jebsen, C., Norici, A., Wagner, H., Palmucci, M., Giordano, M., & Wilhelm, C. (2012). FTIR spectra

of algal species can be used as physiological fingerprints to assess their actual growth potential. *Physiologia Plantarum*, *146*(4), 427–438. https://doi.org/10.1111/j.1399-3054.2012.01636.x

Jiang, H., & Gao, K. (2004). Effects of lowering temperature during culture on the production of polyunsaturated fatty acids in the marine diatom Phaeodactylum tricornutum (Bacillariophyceae). *Journal of Phycology*, *40*(4), 651–654. https://doi.org/10.1111/j.1529-8817.2004.03112.x

Johnson, M. P. (2016). *Photosynthesis An overview of photosynthesis*. *0*, 255–273. https://doi.org/10.1042/EBC20160016

Kim, J. H., Nemson, J. A., & Melis, A. (1993). Photosystem II reaction center damage and repair in Dunaliella salina (green alga): Analysis under physiological and irradiance-stress conditions. *Plant Physiology*, *103*(1), 181–189. https://doi.org/10.1104/pp.103.1.181

Kramer, D. M., & Evans, J. R. (2011). The importance of energy balance in improving photosynthetic productivity. *Plant Physiology*, *155*(1), 70–78. https://doi.org/10.1104/pp.110.166652

Krause, G. H., & Weis, E. (1984). Chlorophyll fluorescence as a tool in plant physiology - II. Interpretation of fluorescence signals. *Photosynthesis Research*, *5*(2), 139–157. https://doi.org/10.1007/BF00028527

Kumari, P., Kumar, M., Reddy, C. R. K., & Jha, B. (2013). Algal lipids, fatty acids and sterols. In *Functional Ingredients from Algae for Foods and Nutraceuticals*. Woodhead Publishing Limited. https://doi.org/10.1533/9780857098689.1.87

Lacour, T., Babin, M., & Lavaud, J. (2020). Diversity in Xanthophyll Cycle Pigments Content and Related Nonphotochemical Quenching (NPQ) Among Microalgae: Implications for Growth Strategy and Ecology. *Journal of Phycology*, *56*(2), 245–263. https://doi.org/10.1111/jpy.12944

Lamers, P. P., Van De Laak, C. C. W., Kaasenbrood, P. S., Lorier, J., Janssen, M., De Vos, R. C. H., Bino, R. J., & Wijffels, R. H. (2010). Carotenoid and fatty acid metabolism in light-stressed Dunaliella salina. *Biotechnology and Bioengineering*, *106*(4), 638–648. https://doi.org/10.1002/bit.22725

Larkum, A. W. D. (2003). *Light-Harvesting Systems in Algae*. https://doi.org/10.1007/978-94-007-1038-2_13

Lavaud, J., & Goss, R. (2014). *The Peculiar Features of Non-Photochemical Fluorescence Quenching in Diatoms and Brown Algae*. 421–443. https://doi.org/10.1007/978-94-017-9032-1_20

Leliaert, F., Smith, D. R., Moreau, H., Herron, M. D., Verbruggen, H., Delwiche, C. F., & De Clerck, O. (2012). Phylogeny and Molecular Evolution of the Green Algae. *Critical Reviews in Plant*

Sciences, *31*(1), 1–46. https://doi.org/10.1080/07352689.2011.615705

LEWIN, J. C. (1958). The taxonomic position of Phaeodactylum tricornutum. *Journal of General Microbiology*, *18*(2), 427–432. https://doi.org/10.1099/00221287-18-2-427

Li, Y., Gu, W., Huang, A., Xie, X., Wu, S., & Wang, G. (2019). Transcriptome analysis reveals regulation of gene expression during photoacclimation to high irradiance levels in Dunaliella salina (Chlorophyceae). *Phycological Research*, *67*(4), 291–302. https://doi.org/10.1111/pre.12379

Lowry. (1951). Lowry Protein Assay. *Journal of Biological Chemistry*.

MacIntyre, H. L., Kana, T. M., Anning, T., & Geider, R. J. (2002). Photoacclimation of photosynthesis irradiance response curves and photosynthetic pigments in microalgae and cyanobacteria. *Journal of Phycology*, *38*(1), 17–38. https://doi.org/10.1046/j.1529-8817.2002.00094.x

Mackinder, L., Miller, T. E., Heuberger, A. L., Peers, G., Smith, K. S., Jonikas, M. C., Grossman, A. R., & Posewitz, M. C. (2014). *Alternative Acetate Production Pathways in Chlamydomonas reinhardtii during Dark Anoxia and the Dominant Role of Chloroplasts in Fermentative Acetate Production*. *26*(November), 4499–4518. https://doi.org/10.1105/tpc.114.129965

Manton, I., & Parke, M. (1965). Observations on the fine structure of two species of Platymonas with special reference to flagellar scales and the mode of origin of the theca. *Journal of the Marine Biological Association of the United Kingdom*, *45*(3), 743–754. https://doi.org/10.1017/S0025315400016568

Mccree, K. J. (1981). *2 Photosynthetically Active Radiation*.

Mitchell, P. (1975). The protonmotive Q cycle: A general formulation. *FEBS Letters*, *59*(2), 137–139. https://doi.org/10.1016/0014-5793(75)80359-0

Montechiaro, F., Hirschmugl, C. J., Raven, J. A., & Giordano, M. (2006). Homeostasis of cell composition during prolonged darkness. *Plant, Cell and Environment*, *29*(12), 2198–2204. https://doi.org/10.1111/j.1365-3040.2006.01593.x

Moreira, D., & Philippe, H. (2001). Sure facts and open questions about the origin and evolution of photosynthetic plastids. *Research in Microbiology*, *152*(9), 771–780. https://doi.org/10.1016/S0923-2508(01)01260-8

Müller, P., Li, X. P., & Niyogi, K. K. (2001). Update on Photosynthesis Non-Photochemical Quenching . A Response to Excess Light Energy 1. *Plant Physiology*, *125*(April), 1558–1566.

Murchie, E. H., & Lawson, T. (2013). Chlorophyll fluorescence analysis: A guide to good practice and understanding some new applications. *Journal of Experimental Botany*, *64*(13), 3983–3998. https://doi.org/10.1093/jxb/ert208

Nagao, R., Ueno, Y., Yokono, M., Shen, J. R., & Akimoto, S. (2019). Effects of excess light energy on excitation-energy dynamics in a pennate diatom Phaeodactylum tricornutum. *Photosynthesis Research*, *141*(3), 355–365. https://doi.org/10.1007/s11120-019-00639-4

Neidhardt, J., Benemann, J. R., Zhang, L., & Melis, A. (1998). Photosystem-II repair and chloroplast recovery from irradiance stress: Relationship between chronic photoinhibition, light-harvesting chlorophyll antenna size and photosynthetic productivity in Dunaliella salina (green algae). *Photosynthesis Research*, *56*(2), 175–184. https://doi.org/10.1023/A:1006024827225

Nelson, N., & Ben-shem, A. (2015). *THE COMPLEX ARCHITECTURE OF OXYGENIC PHOTOSYNTHESIS*. *January*. https://doi.org/10.1038/nrm1525

Niyogi, K. K., & Truong, T. B. (2013). Evolution of flexible non-photochemical quenching mechanisms that regulate light harvesting in oxygenic photosynthesis. *Current Opinion in Plant Biology*, *16*(3), 307–314. https://doi.org/10.1016/j.pbi.2013.03.011

Ogawa, T., Misumi, M., & Sonoike, K. (2017). Estimation of photosynthesis in cyanobacteria by pulse-amplitude modulation chlorophyll fluorescence: problems and solutions. *Photosynthesis Research*, *133*(1–3), 63–73. https://doi.org/10.1007/s11120-017-0367-x

Olaizola, M., La Roche, J., Kolber, Z., & Falkowski, P. G. (1994). Non-photochemical fluorescence quenching and the diadinoxanthin cycle in a marine diatom. *Photosynthesis Research*, *41*(2), 357–370. https://doi.org/10.1007/BF00019413

OLIVEIRA, L., BISALPUTRA, T., & ANTIA, N. J. (1980). Ultrastructural Observation of the Surface Coat of Dunaliella Tertiolecta From Staining With Cationic Dyes and Enzyme Treatments. *New Phytologist*, *85*(3), 385–392. https://doi.org/10.1111/j.1469-8137.1980.tb03177.x

Owens, T. G. (1986). Light-Harvesting Function in the Diatom Phaeodactylum tricornutum . *Plant Physiology*, *80*(3), 739–746. https://doi.org/10.1104/pp.80.3.739

Peers, G., Truong, T. B., Ostendorf, E., Busch, A., Elrad, D., Grossman, A. R., Hippler, M., & Niyogi, K. K. (2009). An ancient light-harvesting protein is critical for the regulation of algal photosynthesis. *Nature*, *462*(7272), 518–521. https://doi.org/10.1038/nature08587

Peltier, G., Tolleter, D., Billon, E., & Cournac, L. (2010). Auxiliary electron transport pathways in chloroplasts of microalgae. *Photosynthesis Research*, *106*(1–2), 19–31. https://doi.org/10.1007/s11120-010-9575-3

Perez-Boerema, A., Klaiman, D., Caspy, I., Netzer-El, S. Y., Amunts, A., & Nelson, N. (2020). Structure of a minimal photosystem I from the green alga Dunaliella salina. *Nature Plants*, *6*(3), 321–327. https://doi.org/10.1038/s41477-020-0611-9

Pisier, G. (2006). Remarks on B (H) ⊗B (H). *Proc. Indian Acad. Sci*, *116*(4), 423–428.

Raven, J.A., 2005. Cellular location of starch synthesis and evolutionary origin of starch genes. *J. Phycol.*, *41*, pp.1070-1072.

Raven, J. A. (2011). The cost of photoinhibition. *Physiologia Plantarum*, *142*(1), 87–104. https://doi.org/10.1111/j.1399-3054.2011.01465.x

Ritchie, R. J. (2006). Consistent sets of spectrophotometric chlorophyll equations for acetone, methanol and ethanol solvents. *Photosynthesis Research*, *89*(1), 27–41. https://doi.org/10.1007/s11120-006-9065-9

Schmidt Nielsen, B., Graves, B., & Roth, J. (1983). Water removal and solute additions determining increases in renal medullary osmolality. *American Journal of Physiology - Renal Fluid and Electrolyte Physiology*, *13*(5). https://doi.org/10.1152/ajprenal.1983.244.5.f472

Sen, B., Kocer, M.A.T. and Alp, M.T., 2005. Studies on growth of marine microalgae in batch cultures: IV. Tetraselmis suecica (Kylin) Butcher (Prasinophyta). *Asian Journal of Plant Sciences*, *4*(6), pp.645-647.

Sharkey, T. D. (2019). Discovery of the canonical Calvin – Benson cycle. *Photosynthesis Research*, *140*(2), 235–252. https://doi.org/10.1007/s11120-018-0600-2

Sharma, K. K., Schuhmann, H., & Schenk, P. M. (2012). High lipid induction in microalgae for biodiesel production. *Energies*, *5*(5), 1532–1553. https://doi.org/10.3390/en5051532

Sheng, X., Watanabe, A., Li, A., Kim, E., Song, C., Murata, K., Song, D., Minagawa, J., & Liu, Z. (2019). Structural insight into light harvesting for photosystem II in green algae. *Nature Plants*, *5*(12), 1320–1330. https://doi.org/10.1038/s41477-019-0543-4

Sui, Y., Muys, M., Vermeir, P., D'Adamo, S., & Vlaeminck, S. E. (2019). Light regime and growth phase affect the microalgal production of protein quantity and quality with Dunaliella salina. *Bioresource Technology*, *275*(December 2018), 145–152. https://doi.org/10.1016/j.biortech.2018.12.046

Taiz, L., & Zeiger, E. (2010). Plant Physiology, Fifth Edition. *Cell*.

Thaipratum, R., Melis, A., Svasti, J., & Yokthongwattana, K. (2009). Analysis of non-photochemical energy dissipating processes in wild type dunaliella salina (green algae) and in zea1, a mutant constitutively accumulating zeaxanthin. *Journal of Plant Research*, *122*(4), 465–476. https://doi.org/10.1007/s10265-009-0229-5

Torzillo, G., Masojídek, J., Kopecky, J., & Koblíz, M. (2004). *The Xanthophyll Cycle in Green Algae (Chlorophyta): Its Role in the Photosynthetic Apparatus*. *6*, 342–349. https://doi.org/10.1055/s-2004-820884

Ubbink, J., & Scha, P. (2003). *The Cell Wall of Lactic Acid Bacteria : Surface Constituents and Macromolecular Conformations*. *85*(December), 4076–4092. https://doi.org/10.1016/S0006-

3495(03)74820-6

Waterborg, J. H., & Matthews, H. R. (1994). The Lowry method for protein quantitation. *Methods in Molecular Biology (Clifton, N.J.)*, *32*(May), 1–4. https://doi.org/10.1385/0-89603-268-x:1

Zhao, R., Cao, Y., Xu, H., Lv, L., Qiao, D., & Cao, Y. (2011). Analysis of expressed sequence tags from the green alga Dunaliella salina (chlorophyta). *Journal of Phycology*, *47*(6), 1454–1460. https://doi.org/10.1111/j.1529-8817.2011.01071.x